JEM Journal of Experimental Medicine

ARTICLE

Competitive fungal commensalism mitigates candidiasis pathology

Jarmila Sekeresova Kralova[1*], Catalina Donic[1*], Bareket Dassa[2], Ilana Livyatan[3], Paul Mathias Jansen[4], Shifra Ben-Dor[2], Lena Fidel[2], Sébastien Trzebanski[1], Lian Narunsky-Haziza[3], Omer Asraf[5], Ori Brenner[6], Hagit Dafni[6], Ghil Jona[2], Sigalit Boura-Halfon[1], Noa Stettner[6], Eran Segal[3], Sascha Brunke[4], Yitzhak Pilpel[5], Ravid Straussman[3], David Zeevi[7], Petra Bacher[8,9], Bernhard Hube[4,10], Neta Shlezinger[11], and Steffen Jung[1]

The mycobiota are a critical part of the gut microbiome, but host–fungal interactions and specific functional contributions of commensal fungi to host fitness remain incompletely understood. Here, we report the identification of a new fungal commensal, *Kazachstania heterogenica* var. *weizmannii*, isolated from murine intestines. *K. weizmannii* exposure prevented *Candida albicans* colonization and significantly reduced the commensal *C. albicans* burden in colonized animals. Following immunosuppression of *C. albicans* colonized mice, competitive fungal commensalism thereby mitigated fatal candidiasis. Metagenome analysis revealed *K. heterogenica* or *K. weizmannii* presence among human commensals. Our results reveal competitive fungal commensalism within the intestinal microbiota, independent of bacteria and immune responses, that could bear potential therapeutic value for the management of *C. albicans*–mediated diseases.

Introduction

The genetic information that defines human beings includes not only the genomes of the human cells but also that of the commensal microbiome. While the analysis of this metagenome has focused mainly on the abundant bacterial commensals (Qin et al., 2010; Coelho et al., 2022), mucosal surfaces are also inhabited by fungi. The role of the mycobiota and their contributions to host fitness are, however, less well understood (Huseyin et al., 2017; Raimondi et al., 2019). This is in part due to the under-representation of fungi in the microbiome of animal models that are kept under strict hygienic conditions (Rosshart et al., 2019; Yeung et al., 2020; Lin et al., 2020).

As one of the most common human fungal pathogens, *Candida albicans* causes hundreds of millions of symptomatic infections each year (Bongomin et al., 2017; Brown et al., 2012). Pathologies are frequently associated with immunodeficiencies and range from superficial irritations of the skin and mucosae to life-threatening invasive infections of internal organs. In addition, chronic mucocutaneous candidiasis has been linked to inborn errors of IL-17 immunity (Cypowyj et al., 2012). Fungal dissemination that leads to systemic infection is believed to originate from the gut where *C. albicans* normally resides as a harmless commensal (Pappas et al., 2018). Candidiasis has been linked to filamentation of the fungus (Noble et al., 2017; Gow et al., 2011), which is strictly associated with the expression of the cytolytic peptide toxin candidalysin that promotes barrier damage (Moyes et al., 2016; Allert et al., 2018). Human individuals are colonized with *C. albicans* in childhood, and clonal fungal populations persist over their lifetime, mostly without symptoms. Emerging evidence suggests that fungal colonization in fact rather benefits than harms the host and that the gut mycobiota improve mammalian immunity (Jiang et al., 2017; Belkaid and Harrison, 2017; Underhill and Iliev, 2014; Wheeler et al., 2016). Specifically, commensal fungi, and in particular *C. albicans*, were shown to affect the composition of the myeloid innate immune compartment (Rosshart et al., 2019; Richardson and Moyes, 2015; Hooper et al., 2012) and elicit cellular and humoral immunity (Conti and Gaffen, 2010; Ost et al., 2021; Doron et al., 2021). Insights not only into the diverse interactions

[1]Departments of Immunology and Regenerative Biology, Weizmann Institute of Science, Rehovot, Israel; [2]Life Sciences Core Facilities, Weizmann Institute of Science, Rehovot, Israel; [3]Molecular Cell Biology, Weizmann Institute of Science, Rehovot, Israel; [4]Department of Microbial Pathogenicity Mechanisms, Leibniz Institute for Natural Product Research and Infection Biology—Hans Knoell Institute Jena (HKI), Jena, Germany; [5]Molecular Genetics, Weizmann Institute of Science, Rehovot, Israel; [6]Veterinary Resources, Weizmann Institute of Science, Rehovot, Israel; [7]Plant and Environmental Sciences, Weizmann Institute of Science, Rehovot, Israel; [8]Institute of Immunology, Christian-Albrecht-University of Kiel, Kiel, Germany; [9]Institute of Clinical Molecular Biology, Christian-Albrecht-University of Kiel, Kiel, Germany; [10]Institute of Microbiology, Friedrich Schiller University, Jena, Germany; [11]The Robert H. Smith Faculty of Agriculture, Food and Environment The Hebrew University of Jerusalem, Rehovot, Israel.

*J. Sekeresova Kralova and C. Donic contributed equally to this paper. Correspondence to Steffen Jung: s.jung@weizmann.ac.il.

of fungi with the mammalian hosts and other fungi but also communication with bacterial commensals could aid our understanding of host physiology. Moreover, a better understanding could allow harnessing the impact of commensal fungi on human immunity for therapeutic purposes. The host–fungi interface remains, however, incompletely understood, not the least due to the lack of suitable experimental animal models and our limited insight into fungal commensalism.

The dominant human fungal commensal, *C. albicans*, has also been reported as part of the mycobiota of mice roaming in the wild (Rosshart et al., 2017, 2019). However, animals kept under specific pathogen–free (SPF) conditions mostly lack *C. albicans* and generally harbor poorly developed mycobiota that also differ considerably between vendors (Mims et al., 2021). Indeed, laboratory mice largely resist *C. albicans* colonization unless subjected to antibiotics (Abx) (Shao et al., 2019), which neutralize inhibiting bacteria, including Lactobacillae (Zangl et al., 2019; Fan et al., 2015).

Here, we report the serendipitous identification of a novel fungal commensal of the *Kazachstania* genus that efficiently colonizes laboratory animals kept in SPF facilities without prior Abx conditioning. The strain, which we termed *Kazachstania heterogenica* var. *weizmannii* (*K. weizmannii*), prevented *C. albicans* colonization, outcompeted *C. albicans* during competitive seeding, and even expelled *C. albicans* from stably colonized animals. Murine hosts mounted comparable humoral, but distinct cellular immune responses to *K. weizmannii* and *C. albicans* exposure, although the latter was not required for the competition phenomenon. Unlike *C. albicans*, non-filamenting *K. weizmannii* did not disseminate or cause pathology in immunosuppressed animals. Rather, interfungal competition that reduced the intestinal *C. albicans* load of mice mitigated fatal candidiasis. Finally, human metagenome analysis revealed *K. heterogenica* or *weizmannii* as a component of the commensal intestinal and vaginal microbiota. Taken together, we report robust competitive commensalism between fungi of the *Kazachstania* and *Candida* clades, which can mitigate systemic fungal pathology, as shown for candidiasis in mice.

Results

Identification of a novel commensal fungus in laboratory mice

To probe for the role of myeloid cells in antifungal immunity, we generated mice that harbor a deficiency of the cytokine IL-23 and attempted to colonize them with *C. albicans*. Specifically, we used a protocol involving prior conditioning of animals with Abx (Shao et al., 2019) (Fig. 1 A). Ampicillin-exposed wild-type (WT) mice could be readily and persistently seeded with *C. albicans* SC5314 harboring a GFP reporter (Gonia et al., 2017) (Fig. 1 B). However, we consistently failed to efficiently colonize the *Il23a*$^{\Delta/\Delta}$ mice with *C. albicans* (Fig. 1 C). Following the plating of the fecal microbiota of these animals, we noted the growth of another yeast-like fungus of distinct morphology (Fig. 1, D and E). Sequencing of DNA isolated from the plated fungus using the internal transcribed spacer (ITS) as yeast barcode (Schoch et al., 2012) tentatively identified the fungus as a member of the *Kazachstania* clade (Fig. S1, A and B). This genus is composed of over 50 species found in both anthropic and non-anthropic environments and associated with sourdough production (Kurtzman et al., 2005; Arora et al., 2020). Whole-genome sequencing of the new fungus revealed the characteristic gene duplications of the Saccharomycetaceae family and established it as a novel *Kazachstania* strain. Phylogenetic analysis of 26S rDNA confirmed the assignment of the fungus to the Saccharomycetaceae clade (Fig. 1 F), and comparison to other *Kazachstania* species (Fig. 1 G) placed it together with *K. heterogenica*, a fungus found in rodent feces, and in a sister clade with *Kazachstania pintolopesii*. We decided to term the new fungus *K. heterogenica* var. *weizmannii*, or *K. weizmannii* for short. Comparison of the *K. weizmannii* genome with other full-length *Kazachstania* genomes (Fig. 1 H) showed that *K. heterogenica* is the closest species, followed by *K. pintolopesii*, *Kazachstania telluris*, and *Kazachstania bovina* in the *K. telluris* complex. Of note, although we originally discovered the novel *Kazachstania* species in *Il23a*$^{\Delta/\Delta}$ mice that could have impaired antifungal immunity, sentinel screening in our animal facilities with the ITS assay revealed that *K. weizmannii* was widespread, irrespective of genotypes of the animals.

In vitro characterization of *K. weizmannii*

When cultured in a number of defined conditions frequently found in the human body, such as serum exposure, neutral pH and/or 37°C, *C. albicans* forms hyphae (Noble et al., 2017). The same challenges did not invoke hyphenation in *K. weizmannii*, but the fungus continued to grow with yeast-like morphology (Fig. 2 A).

Comprehensive Biolog analysis (Data S1) revealed differential preferences for carbon and nitrogen sources of *C. albicans* and *K. weizmannii* (Fig. 2, B and C). *K. weizmannii* was, for instance, superior in growing with 2-deoxy-D-ribose and D-glucosamine, as well as leucine dipeptides. Conversely, *C. albicans* thrived better on maltose, D-galactose, urea, and glycine dipeptides. The two fungi also displayed differential resistance to chemical inhibitors (Fig. 2 D). Specifically, *K. weizmannii* showed, as compared with *C. albicans*, relative resistance to propiconazole and fluconazole, while the yeast was more sensitive to chlorides and bromides. When cultured in SD media, *C. albicans* and *K. weizmannii* displayed similar pH optima (Fig. 2 E). Cultures under different temperatures revealed that both *K. weizmannii* and *C. albicans* grew at 37°C, while in line with it being a pathogen, *C. albicans* was superior in tolerating higher temperatures (Fig. 2 F, Fig. S1 C, and Data S2).

Interestingly and in contrast to the observation for the gut, *C. albicans* and *K. weizmannii* grew in in vitro yeast extract–peptone–dextrose (YPD) cocultures together without interference (Fig. 2 G and Fig. S1 D). Under the condition tested, competition between the strains was hence restricted to the gut environment.

K. weizmannii is a murine commensal that antagonizes *C. albicans* colonization

To facilitate the comparative analysis of *K. weizmannii* and *C. albicans* SC5314, we generated a *K. weizmannii* strain harboring a gene encoding a red fluorescent miRFP reporter (Zahradník et al., 2021) in the enolase 1 (*ENO-1*) locus, mimicking the *C. albicans* SC5314-GFP configuration (Fig. 3 A and Fig. S2, A and B).

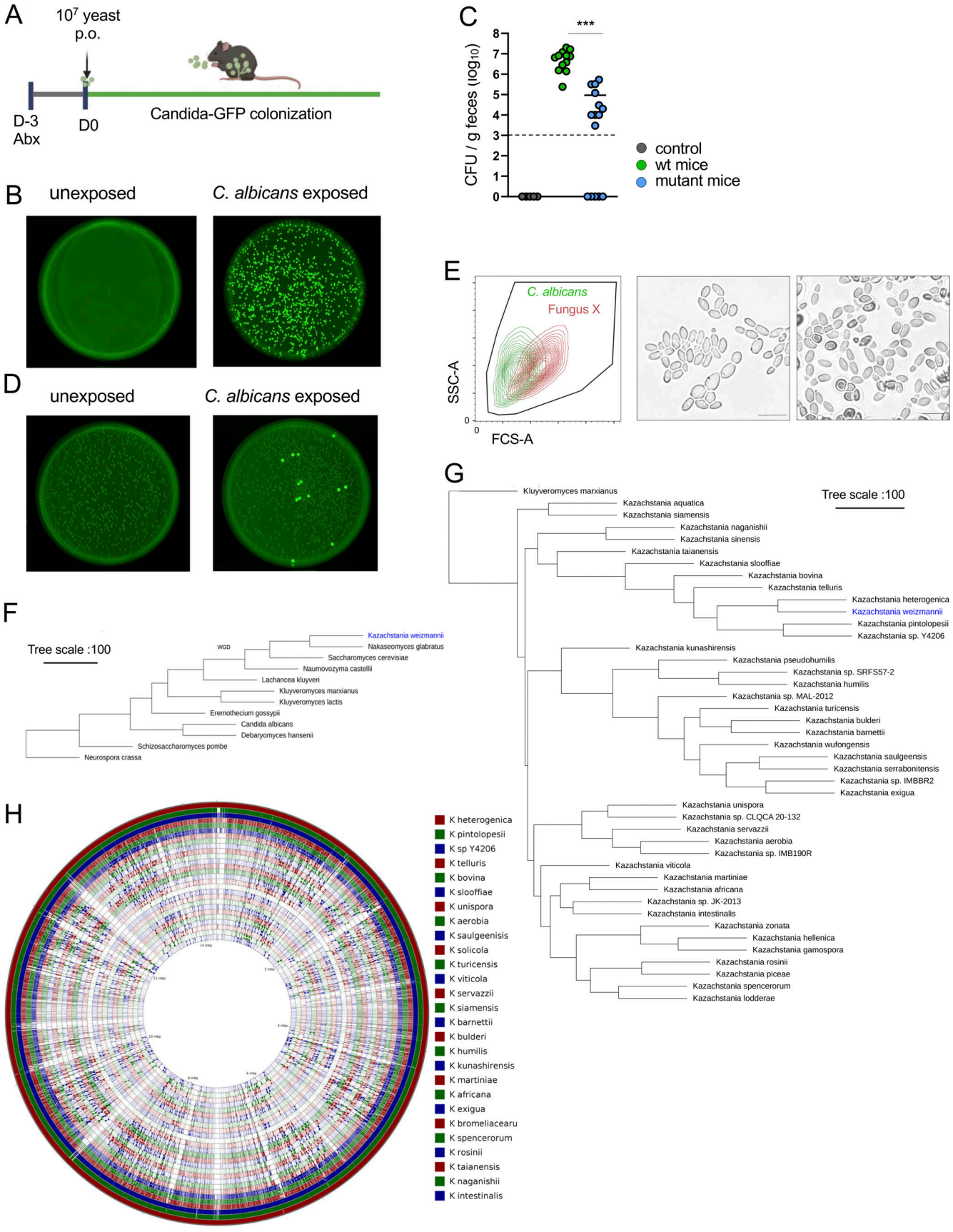

Figure 1. **Identification and characterization of *K. weizmannii*. (A)** Schematic of *C. albicans* colonization protocol, adopted from Basu et al. (2000). **(B)** Recoverable *C. albicans* in the feces of WT mice with Abx supplementation in the drinking water, 2 wk after oral *C. albicans* inoculation. The corresponding

statistical analysis shows mean, and significance is calculated in two-tailed Student's *t* test. **(C)** Recoverable *C. albicans* GFP colonies in feces of unexposed WT (controls), *C. albicans* inoculated mutant mice, and WT animals. Stippled line, limit of detection; *t* test = 0.0001 WT vs. mutant *Candida* colonization. **(D)** Recoverable *C. albicans–GFP* in the feces 2 wk after oral inoculation. Comparison of unexposed and *Candida*-inoculated mutant animals. **(E)** Flow cytometry and microscopical examination of fungal colonies recovered from mutant animals. Scale bars represent 10 µm. **(F)** Phylogenetic tree based on maximum parsimony of the 26S rDNA domains 1 and 2 (D1/D2) region of newly identified *K. weizmannii* in comparison to other yeast model species. **(G)** Phylogenetic tree based on maximum parsimony of the 26S rDNA D1/D2 region of *K. weizmannii* in comparison to other *Kazachstania* species. **(H)** Comparison of the whole genome of newly identified *K. weizmannii* to whole genomes of 27 *Kazachstania* species. *** P ≤ 0.001.

Colonization of WT animals by *K. weizmannii* did not require prior Abx treatment, in contrast to the colonization with *C. albicans* in our facility (Fig. 3, B and C). C57BL/6 mice could be readily colonized by oral *K. weizmannii* inoculation or cohousing with animals bearing the fungus. Interestingly, and in line with our original observation, when Abx-treated mice were co-inoculated with a 1:1 mixture of *K. weizmannii* and *C. albicans*, *Candida* colonization was prevented (Fig. 3, D–G). Robust and rapid out-competition of *C. albicans* by *K. weizmannii* in this assay was confirmed by specific genomic PCR analysis of feces of respective coinoculated animals (Fig. 3 H). The competition was also observed with *K. heterogenica*, the yeast closest to *K. weizmannii* (Fig. 3 I). Of note, competition was not restricted to *C. albicans*, but *K. weizmannii* coinoculation also inhibited colonization with *Candida parapsilosis*, an emerging fungal pathogen (Branco et al., 2023), but it did not interfere with *Candida glabrata* colonization (Fig. 3 J).

To test if *K. weizmannii* would also outcompete established commensal *C. albicans*, we stably colonized mice with *C. albicans* (on Abx) and then cohoused the animals with mice harboring *K. weizmannii*, maintaining Abx exposure (Fig. 3 K). Coprophagy led to the progressive rapid ousting of *C. albicans* by *K. weizmannii*, leaving only a residual *C. albicans* population, which was further reduced upon Abx withdrawal (Fig. 3 L and Fig. S2 C).

C. albicans colonization of mice is sensitive to the microbiome composition (Graf et al., 2019; Alonso-Roman et al., 2022). The observed competition between the two fungi could hence be due to alterations in the bacterial landscape. Comparison of the microbiome of *K. weizmannii*–colonized mice and non-colonized controls using 16S sequencing revealed, however, only minor consistent changes (Fig. S3 A). Moreover, also the abundance of Lactobacillae that are known to impede *C. albicans* colonization of the murine gut (Zangl et al., 2019) was unaltered (Fig. S3 B). To further probe the potential involvement of bacterial microbiota in the fungal competition, we orally inoculated germ-free animals with a mixture of the two fungi. Also in these mice, *K. weizmannii* prevented efficient *C. albicans* colonization (Fig. 3 M and Fig. S3, C–F).

Collectively, these data establish that *K. weizmannii* can outcompete *C. albicans* including previously colonized animals, that the observed inter-fungal competition can be observed for other members of the *Kazachstania* and *Candida* clades, and that it is independent of bacterial microbiome components.

Comparative analysis of the host immune response to *C. albicans* and *K. weizmannii*

Fungi are known to affect host granulopoiesis (Basu et al., 2000) and induce both humoral and cellular immunity (Ost et al., 2021; Leonardi et al., 2022). In line with these reports, Abx-treated animals colonized with *C. albicans* showed an expanded blood neutrophil compartment. In contrast, *K. weizmannii*–colonized animals displayed no significantly altered abundance of granulocytes, classical or non-classical monocytes (Fig. 4 A).

Intestinal IgA responses to *C. albicans* were proposed to balance commensalism vs. pathogenicity by controlling the critical morphological yeast-to-hyphae transition of the fungus (Ost et al., 2021). To assess humoral immunity against the two fungal commensals, we analyzed the sera of colonized animals for reactivity to cultured *K. weizmannii* or *C. albicans*. Colonization with either yeast induced robust anti-fungal serum IgA or IgG titers in most animals (Fig. 4, B and C; and Fig. S3 G). The induced antibodies were mostly, but not always, crossreactive between the two fungal species; however, they did not bind *Saccharomyces cerevisiae* in the assay (Fig. S3 H).

Mucosa-associated fungi, specifically *C. albicans*, have been shown to induce Th17-type cellular immune response (Hernández-Santos and Gaffen, 2012; Leonardi et al., 2022). Accordingly, *C. albicans*–colonized animals displayed an expansion of Th17 cells in gut mucosa–associated mesenteric and peripheral lymph nodes (Fig. 4, D and E). In contrast, even after extended colonization, no Th17 cell expansion was observed in *K. weizmannii*–colonized animals. We also did not observe significant alterations of the Th1 compartment in the lymph node analyzed with this assay, which however does not screen for antigen-specific cells (Fig. 4 E).

With the above, we establish that colonized mice respond to the fungi, although the rapid out-competition we observe (Fig. 3 H) suggests that the phenomenon is independent of adaptive cellular or humoral immunity. To directly test for the potential role of B and T cells in the *Kazachstania/Candida* competition, we investigated colonization in lymphocyte-deficient *Rag2*$^{-/-}$ mice. *K. weizmannii* prevented *C. albicans* colonization also in these lymphocyte-depleted animals (Fig. 4 F).

To directly gauge the impact of *K. weizmannii* on host cells, we performed an epithelial cell (EC) coculture assay (Allert et al., 2018). EC exposure to *C. albicans* resulted in EC damage as measured by lactate dehydrogenase (LDH) release. In contrast and similar to coculture with *S. cerevisiae*, *K. weizmannii* did not affect EC viability (Fig. 4 G and Data S3). However, coinfection of EC cultures with *K. weizmannii* and *C. albicans* did also not prevent EC damage.

Taken together, colonization of Abx-treated animals with both *C. albicans* and *K. weizmannii* induced largely crossreactive humoral immune responses reflected by serum IgA and IgG titers. The characteristic antifungal Th17 response was restricted to *C. albicans*–colonized mice; however, the fungal competition we observed was independent of adaptive immunity. In combination with the results obtained from in vitro EC cocultures,

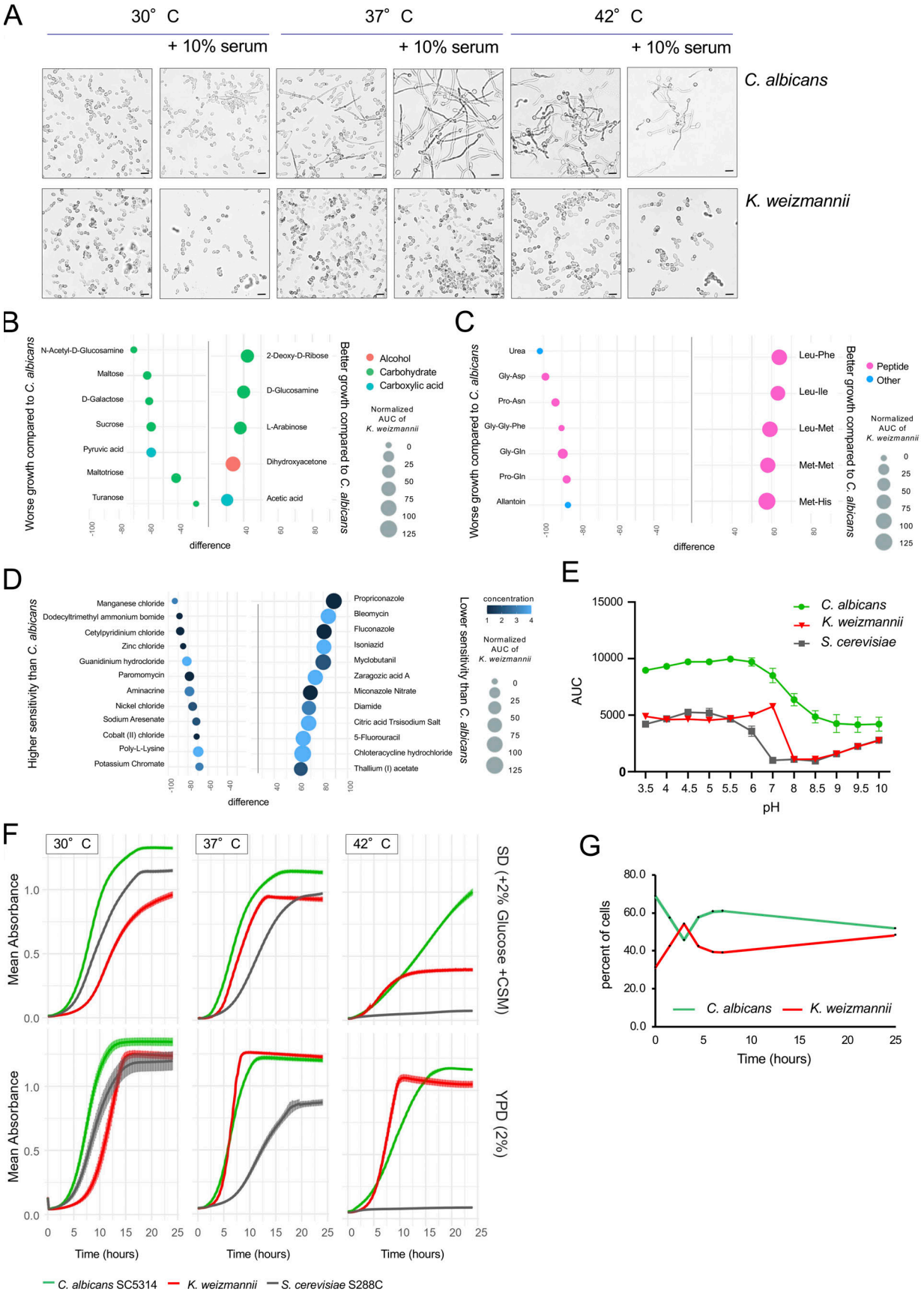

Figure 2. **In vitro culture characteristics of *K. weizmannii*. (A)** Representative images of *C. albicans* and *K. weizmannii* in liquid media in the presence of filament-inducing conditions; *n* = 3 independent experiments. Scale bars represent 10 µm. **(B)** Graph showing the largest differences in growth between

K. weizmannii and *C. albicans* with different carbon sources, based on a z-score > or <2. Differences were calculated using the normalized AUC of *K. weizmannii* and *C. albicans*. Normalization of the AUC based on the growth of both species with glucose. Size of data points corresponds to the normalized AUC of *K. weizmannii* with the corresponding carbon source. All measurements were done using the Biolog PMs in biological triplicates. X axis represents the difference in AUC between *K. weizmannii* and *C. albicans*, while the y axis shows the different carbon sources tested. The data points are color-coded according to the different types of carbon sources. **(C)** Graph showing largest differences in growth between *K. weizmannii* and *C. albicans* with different nitrogen sources, based on a z-score > or <2. Differences were calculated using AUC of *K. weizmannii* and *C. albicans*. normalized based on the growth of both species with glutamine. Size of data points corresponds to the normalized AUC of *K. weizmannii* with the corresponding nitrogen source. All measurements were done using the Biolog PMs in biological triplicates. X axis represents the difference in AUC between *K. weizmannii* and *C. albicans*, while the y axis shows the different nitrogen sources tested. The data points are color-coded according to the different types of nitrogen sources. **(D)** Plot of the largest differences in growth of *K. weizmannii* and *C. albicans* with different inhibitors to test their chemical sensitivity. Graph shows the largest differences in growth between *K. weizmannii* and *C. albicans* with different inhibitors, based on a z-score > or <2, calculated using AUC of *K. weizmannii* and *C. albicans*. AUC normalization was based on the growth of both species without any inhibitor at pH 5. The size of each data point corresponds to the AUC of *K. weizmannii* with the corresponding inhibitor. All measurements were done using the Biolog PMs for chemical sensitivity (PM21-PM25) in biological triplicates. **(E)** Growth curves of *C. albicans*, *S. cerevisiae*, and *K. weizmannii* under different pH conditions in YPD medium. **(F)** Growth curves of *C. albicans*, *S. cerevisiae*, and *K. weizmannii* under different temperatures in SD medium (+2% glucose + CSM) and YPD, biological triplicates. **(G)** Co-culture assay of *C. albicans* and *K. weizmannii* in liquid YPD medium. GFP expressing *C. albicans* was detected by flow cytometry to discriminate between fungi; *n* = 2 independent experiments.

these data furthermore suggest that *K. weizmannii* is in mice an innocuous commensal.

Commensal *C. albicans*, but not *K. weizmannii*, causes pathology in immunosuppressed animals

Invasive candidiasis is widely recognized as a major cause of morbidity and mortality in the healthcare environment, often associated with an underlying immunocompromised state (Pappas et al., 2018; Iliev and Leonardi, 2017). Candidiasis can be induced in otherwise resistant, orally *C. albicans*–challenged animals by immunosuppression (Solis and Filler, 2012). To test whether corticosteroid treatment would cause *C. albicans* and *K. weizmannii* to spread from established commensal reservoirs and cause systemic pathology, we treated mice that were stably colonized with the respective fungi with cortisone 21-acetate boli (225 mg/kg s.c.) every other day (Fig. 5 A). Unlike non-colonized control mice, *C. albicans*–harboring animals lost significant weight after 1 wk of treatment and became moribund (Fig. 5 B). Animals displayed prominent tongue candidiasis and fungal growth in the kidneys (Fig. 5, C and D). In stark contrast, immunosuppressed animals colonized with *K. weizmannii* showed neither weight loss nor evidence of fungal spread (Fig. 5, E–I; and Fig. 4, A and B). These data corroborate reports from the clinic (Pappas et al., 2018) and mouse models (Sprague et al., 2022) that gut commensal *C. albicans* is a pathobiont and can be the source of candidiasis. Furthermore, they establish that in mice, *K. weizmannii* is innocuous, and even in immunosuppressed animals neither breaches the intestinal barrier to spread systemically nor causes pathology.

Competitive commensalism mitigates candidiasis

Since *K. weizmannii* exposure during competitive seeding and cohousing significantly reduced the commensal *C. albicans* burden in colonized animals (Fig. 3 J), we next asked whether this commensal competition could mitigate candidiasis pathology. To simplify the mode of *Kazachstania* administration, we treated *C. albicans*–colonized animals with *Kazachstania*-supplemented drinking water (Fig. 6 A) prior to immunosuppression. As expected, also in this setting, *K. weizmannii* efficiently expelled *C. albicans* from colonized animals (Fig. 6, B and C). Exposure of immunosuppressed *C. albicans*–colonized animals to *K. weizmannii* significantly delayed the weight loss and systemic yeast spread, as indicated by the absence of kidney colonization (Fig. 6, C–F, and Fig. S4 B). Notably, though, the animals were not permanently protected as residual commensal *C. albicans* eventually disseminated and caused pathology (Fig. 6 G and Fig. S4, C and D).

Collectively, these results establish that *K. weizmannii* outcompetes *C. albicans* from the commensal microbiome by reducing the cause of pathology, mitigates candidiasis, and improves the health status of immunosuppressed animals.

Kazachstania presence in human microbiomes

Candida species are a major component of the human mycobiota, with *C. albicans* being the most prevalent (Nash et al., 2017). Despite their established role in dough fermentation (Arora et al., 2020), *Kazachstania* spp. presence in healthy humans or during pathology-associated dysbiosis has rarely been reported (Ling et al., 2021; Wang et al., 2020). Accordingly, a recent study of human mucosa–associated mycobiota showed that these fungi are sparse among human commensals (Leonardi et al., 2022). To gauge the abundance of *Kazachstania* spp. in human microbiota, and specifically *K. heterogenica* or *K. weizmannii* (*K.h/w*), for which we showed the *Candida* competition in mice, we designed a bioinformatic screen to detect genomic regions specific to these fungi out of shotgun sequence information from a collection of 13,174 published metagenomics data sets (Coelho et al., 2022) (Fig. S5). Among 7,059 human gut metagenome samples analyzed, we identified a few hundred samples that harbored ITS sequences of either the genus *Kazachstania* (i.e., with 9,236 read assemblies of 25s ribosomal RNA [rRNA]) or *Candida* (7,167 reads), or both (Fig. 7 A). Among these, 32 metagenomes displayed specific evidence for *K.h/w* (20 unique to *K.h/w* and 12 shared with both species, listed in Fig. S5). Likewise, among 173 vaginal metagenomes analyzed, we found 22 samples with evidence for *Kazachstania* spp. and *Candida* spp. sequences, including five indicating the specific presence of *K.h/w* (Fig. 7 B and Fig. S5). *K.h/w*-positive samples had a wide range of biogeographical distribution (Tables S5 and S6). Collectively, our data support the notion that *K.h/w* can be part of the human microbiome.

To further investigate the relative distribution of *Candida* and *Kazachstania* species in the human microbiome, we performed a

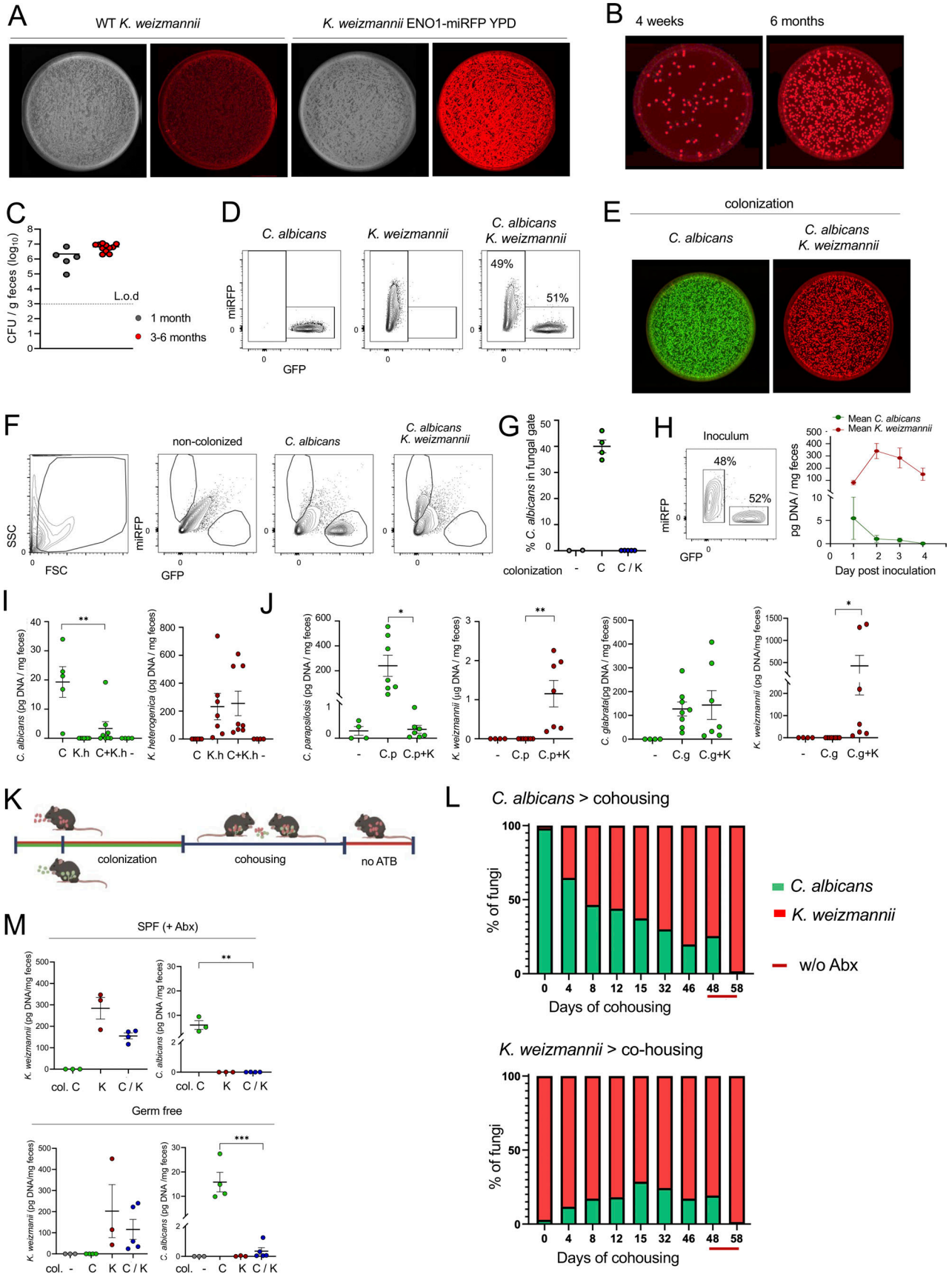

Figure 3. ***K. weizmannii* competition with *C. albicans* in colonized animals. (A)** Far-red fluorescent reporter *Kazachstania* strain (*K. weizmannii* ENO1-miRFP). Representative picture. **(B and C)** Recoverable fecal *K. weizmannii* in colonized WT animals (kept without Abx) 1 and 6 mo after single oral *K. weizmannii*

ENO1-miRFP inoculation. **(D)** Flow cytometric analysis of *C. albicans* SC5314 (ENO1-GFP), *K. weizmannii* (ENO1-miRFP), and mixed cultures used for oral inoculation (E). **(E)** Representative plating analysis of feces of animals inoculated with 10^7 yeasts of *C. albicans* SC5314 (ENO1-GFP) or *K. weizmannii* (ENO1-miRFP), and mixed cultures (see D) 3 wk after administration. **(F and G)** Flow cytometric analysis of feces of animals orally inoculated with 10^7 yeasts of *C. albicans* SC5314 (ENO1-GFP), *K. weizmannii* (ENO1-miRFP), and mixed cultures (see D) 3 wk after administration. Quantification (n = 3–5 mice per group, four independent experiments). **(H)** Flow cytometric analysis of a mixed culture used for oral inoculation (right) and quantitative PCR analysis of genomic DNA of *C. albicans* and *K. weizmannii* recovered daily from feces of SPF animals colonized with a 1:1 mixture. Data shown as mean DNA quantities per mg of feces of N = 5 Abx-treated mice; error bars represent SEM. **(I)** Quantitative PCR analysis of genomic DNA of *C. albicans* SC5314 and *K. heterogenica* recovered from feces of SPF animals colonized with either *C. albicans* SC5314 (C), *K. heterogenica* (K.h) or mixed culture (C+K.h) compared to Abx-treated SPF animals (–) 1 wk after administration; n = 2–4 mice per group; two independent experiments; data shown as mean ± SEM, statistical significance calculated using ANOVA, $P < 0.05$. **(J)** Quantitative PCR analysis of genomic DNA of *C. parapsilosis, C. glabrata*, and *K. weizmannii* recovered from feces of SPF animals colonized with either *C. parapsilosis* (C.p), *C. glabrata* (C.g), or mixed culture (C.p+K, C.g+K) compared to Abx-treated SPF animals (–) 1 wk after administration; n = 2–4 mice per group; two independent experiments; data shown as mean ± SEM, statistical significance calculated using ANOVA, $P < 0.05$. **(K)** Schematic of co-housing experiment. **(L)** Percentages of the respective labeled fungi in feces of *C. albicans*, *K. weizmannii* colonized animals, before and after co-housing in Abx presence (except for day 48 and 58); Abx withdrawal on day 46 of cohousing, n = 4 per group, representative of two independent experiments. **(M)** Quantitative PCR analysis of genomic DNA of *C. albicans* SC5314 and *K. weizmannii* recovered from feces of germ-free animals colonized with *C. albicans* SC5314 (C), *K. weizmannii* (K), or mixed culture (C/K) compared with Abx-treated SPF animals (–) 1 wk after administration; n = 3–4 mice per group; representative of two independent experiments; data shown as mean ± SEM, statistical significance calculated using ANOVA, $P < 0.05$. * $P \le 0.05$, ** $P \le 0.01$, *** $P \le 0.001$.

sensitive ITS2 analysis of fecal samples of a cohort of 570 healthy individuals (Zeevi et al., 2019; Korem et al., 2017) (Fig. 7 C and Table S7). Since the *Kazachstania* genus had not been widely detected in prior ITS2 sequencing initiatives (Nash et al., 2017), we anticipated that it would be a less prevalent genus with lower abundance when compared with *Candida* and other prominent genera. Therefore, we added empty control samples which underwent the same amplification and library preparation processes to enable the application of a novel ITS2 processing pipeline previously applied to analyze the low biomass environment of the tumor mycobiome (Narunsky-Haziza et al., 2022). Indeed, 13 fungal species could be detected in control samples with read numbers ranging from 1 to 100 reads per species per sample. We, therefore, applied an aggressive cutoff by flooring all species that obtained <100 reads in a given sample to zero in that sample. This process yielded 215 samples with ITS2 sequence evidence of either *Candida* or *Kazachstania* species. *C. albicans* was the most prominent *Candida* species found in 120 samples, followed by *C. parapsilosis* and *C. tropicalis*, with 29 and 15 samples, respectively. Two *Kazachstania* species were detected across 37 samples prior to flooring and were completely absent from negative control samples. Still, these species were floored in samples where they did not reach 100 reads leaving 12 samples with *Kazachstania servazii* and three samples with *Kazachstania exigua*. Potentially due to its limited size, we did not detect *K.h/w* specifically in this cohort.

Finally, we corroborated *Kazachstania* presence in the human microbiome by antigen-reactive T cell enrichment (ARTE) analysis (Bacher et al., 2013) of peripheral blood of a limited number of healthy individuals. ARTE revealed T cell reactivity directed against *C. albicans* extracts, as shown earlier (Bacher et al., 2019), but also against *K. weizmannii* (Fig. 7 D). *C. albicans*–reactive T cells were polarized toward IL-17– and IL-22–producing Th17 fates. In contrast, *K. weizmannii*–reactive T cells were IFNγ-producing Th1 type cells, like T cells that reacted to *S. cerevisiae*. Of note, $CD154^+$ memory T cells responsive to the Saccharomycetaceae extracts also expressed β7 integrin indicative of their generation in the gut mucosa (Gorfu et al., 2009).

Collectively, these data establish *Kazachstania* spp. and specifically *K. heterogenica* and *weizmannii*, for which we show the activity to compete with *C. albicans* in the animal model, as part of the human commensal microbiome.

Discussion

Here, we report the identification of a new fungal commensal of mice and human intestines. Unlike the well-studied *C. albicans*, *K. weizmannii* readily colonized animals kept under SPF conditions without prior Abx conditioning. Moreover, *K. weizmannii* efficiently outcompeted *C. albicans* when coinoculated and also reduced the intestinal *C. albicans* load of previously colonized animals. Furthermore, competitive commensalism mitigated candidiasis pathology in mice under immune suppression.

Commensal mycobiota are understudied and rarely appreciated as a critical, active part of the microbiota. Noteworthy exceptions include emerging evidence for the role of *C. albicans* in shaping Th17 immunity, behavior, and potential cancer progression (Leonardi et al., 2022; Narunsky-Haziza et al., 2022; Dobeš et al., 2022). One of the reasons that commensal fungi have gained less attention than prokaryotes is the fact that, unlike mice roaming in the wild (Rosshart et al., 2017), animals kept under hyper-hygienic SPF conditions harbor poorly developed commensal mycobiota. Moreover, the study of fungi has primarily focused on *C. albicans*, but colonization of laboratory animals with this human pathobiont is impeded by bacterial communities, such as Lactobacillae (Fan et al., 2015; Zangl et al., 2019) and therefore requires Abx conditioning (Shao et al., 2019).

K. weizmannii colonizes SPF mice without prior Abx conditioning and is hence, unlike *C. albicans*, resistant to bacterial commensals that impede fungal growth in SPF colonies (Fan et al., 2015; Zangl et al., 2019). The mechanisms that underlie the competition of Lactobacillae with *C. albicans* are manifold and include toxic metabolic products, biofilm interference, physical interactions, and forced metabolic adaptation that compromises the pathogenicity of *C. albicans* (Zangl et al., 2019; Graf et al., 2019). Likewise, the mechanism that underlies competitive commensalism between *K. weizmannii* and *C. albicans* in mice might be complex. The Biolog analysis for in vitro growth requirements revealed the preferences of the respective

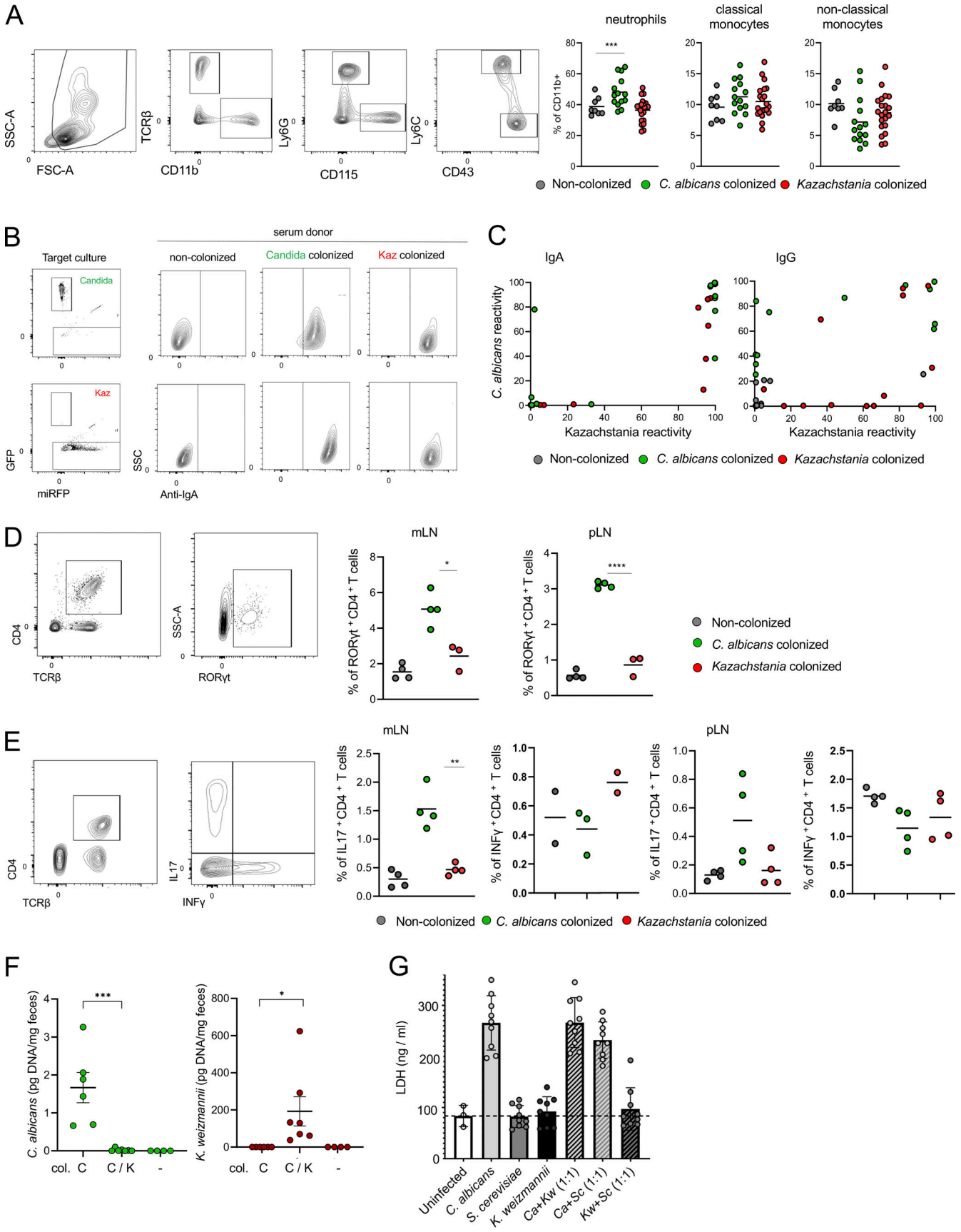

Figure 4. **Humoral and cellular immune responses to *C. albicans* and *Kazachstania* sp. (A)** Flow cytometric analysis of myeloid blood cell compartment of mice 4 wk colonized with *C. albicans* or *K. weizmannii*. Neutrophils, classical, and non-classical monocytes are defined as Ly6G$^+$ CD115$^-$, Ly6C$^+$ CD115$^+$, and

Ly6C⁻ CD115⁺ cells, respectively. *N* = 8–21 mice, pooled from three independent experiments. Gating strategy, left; results, right. The corresponding statistical analysis shows mean; significance is calculated with two-tailed Student's *t* test. **(B)** Flow cytometric analysis of humoral anti-fungal reactivity. Gating strategy for the determination of serum immunoglobulin binding to cultured *C. albicans* or *K. weizmannii*. **(C)** Anti-*C. albicans* and *K. weizmannii* IgA and IgG serum reactivity of single-colonized animals, measured as shown in B. Note that most but not all animals harbor cross-reactive sera. Data shown as percentage of Ig-positive gate, two pooled independent experiments, *N* = 11–13 per group. **(D)** Representative gating strategy of RORγt⁺ T cells (left); percentage of RORγt⁺ cells among TCRβ CD4⁺ T cells 1 mo following *C. albicans* or *K. weizmannii* colonization, *n* = 3–5 mice per group, three independent experiments (right). The corresponding statistical analysis shows mean; significance is calculated with two-tailed Student's *t* test. **(E)** Representative gating strategy of IL17 producing Th17 cells (left); percentage of IL17⁺ cells among TCRβ CD4⁺ T cells 1 mo following *C. albicans* or *K. weizmannii* colonization, *n* = 3–5 mice per group, three independent experiments (right). The corresponding statistical analysis shows mean; significance is calculated with two-tailed Student's *t* test. **(F)** Quantitative PCR analysis of genomic DNA of *C. albicans* SC5314 and *K. weizmannii* recovered from feces of *Rag2*$^{-/-}$ animals colonized with *C. albicans* SC5314 (C) or a mixed culture (C/K) compared to Abx-treated SPF animals (–) 1 wk after administration; *n* = 3–4 mice per group, pooled two independent experiments; data shown as mean ± SEM; statistical significance calculated using ANOVA, $P < 0.05$. **(G)** EC coculture assay of *C. albicans*, *S. cerevisiae*, and *K. weizmannii*. EC damage was assessed using the LDH assay as described in Allert et al. (2018). * $P \le 0.05$, ** $P \le 0.01$, *** $P \le 0.001$, **** $P \le 0.0001$.

fungi for specific carbon and nitrogen sources. Carbon and nitrogen catabolite metabolism has been discussed in the context of virulence of human pathogenic fungi (Ries et al., 2018). Whether the growth condition differences between *K. weizmannii* and *C. albicans* translate to the competition of the two fungi in the murine gut requires however further study.

The results of the 16S analysis suggest that *K. weizmannii* does not significantly alter the bacterial microbiome composition of the host. However, the fungus might impact the fecal metabolomic landscape (Guo et al., 2017) by altering bacterial expression profiles. Gastric *C. albicans* colonization of mice was shown to be affected by diet (Yamaguchi et al., 2005). Moreover, the fungal microbiome, including *Kazachstania* spp., was recently reported to be modulated by dietary intervention in pigs (Xu et al., 2023). The identification of *K. weizmannii* as a murine fungal commensal that colonizes mice in the presence of bacteria should help to explore the impact of the fecal procaryotic metabolome on mycobiota, their interactions, as well as the potential to manage colonization with pathobionts.

When cohoused with *K. weizmannii*–bearing animals, mice under Abx treatment that are colonized with *C. albicans* progressively lose the pathobiont from the fecal microbiome. The residual *C. albicans* population is even further reduced upon Abx withdrawal. This finding might suggest the existence of two separate compartments in the intestine of mice: a fecal niche in which the fungi compete and an epithelia-associated niche which in SPF mice is dominated by commensal bacteria that prevent colonization by *C. albicans*, but not by *K. weizmannii*.

Following immunosuppression of colonized animals, *C. albicans* can breach the intestinal barrier (Vautier et al., 2015), an activity that requires filamentation (Felk et al., 2002), as well as expression of the cytolytic peptide toxin candidalysin that promotes invasion of the EC layer (Allert et al., 2018). In contrast, *K. weizmannii* remains confined to the gut lumen, in line with the observation that *K. weizmannii* does not form filaments upon in vitro stress, and the fungus lacks part of the Core Filamentation Response Network identified in *C. albicans* (Martin et al., 2013).

We identified *K. weizmannii* by serendipity in mice that harbor impaired Th17 immunity; in line with its ability to colonize WT SPF mice without Abx conditioning, *K. weizmannii* was however widely spread in our animal facility, irrespective of the genotypes. Moreover, our metagenome screen yielded evidence that *K. weizmannii* is also part of human intestinal and vaginal microbiomes. To date, reports of *Kazachstania* spp. are largely related to its involvement in food fermentation (Arora et al., 2020), while associations with murine or human commensalism or dysbiosis remain rare (Wang et al., 2020; Leonardi et al., 2022). It remains therefore unclear why the fungus so far escaped the radar. Rarefaction curves indicate that a cohort of 200 human samples is sufficient to comprehensively detect the human mycobiome taxonomic content, and our improved analysis pipeline pinpoints *Kazachstania* spp. as members. Yet, we observed that many members of the stool mycobiome, including *Kazachstania* spp., are masked by *S. cerevisiae* abundance and other food-related fungi. Only the arduous following of a serendipitous observation and the focus on a particular genus enabled our finding. Notably, the majority of individuals harboring *Kazachstania* species in the local cohort displayed mutual exclusive presence with *Candida* spp. suggesting competitive fungal commensalism, as in mice. However, the notion of inverse correlation of these fungi and *Candida* spp. warrants further studies on a larger scale, since the sparsity of *Kazachstania* spp. precludes statistical significance.

Taken together, we identified with *K. weizmannii* an innocuous fungal commensal in men and mice. By its virtue of successfully competing with *C. albicans* in the murine gut for to-be-defined niches, *K. weizmannii* lowered the pathobiont burden and mitigated candidiasis development in immunosuppressed animals. This competitive fungal commensalism we report for members of the *Kazachstania* and *Candida* clades could have potential therapeutic value for the management of *C. albicans*–mediated diseases.

Materials and methods

Mice

All animals involved in this study, unless otherwise noted, were of C57BL/6 background and of adult age (6–12 wk). Mutant *Il23a*$^{\Delta/\Delta}$ mice were generated by crossing *Il23a*$^{fl/fl}$ animals (Thakker et al., 2007) to *Pgk*^{Cre} mice (Lallemand et al., 1998). Unless indicated otherwise, animals were maintained in a SPF facility with chow and water provided ad libitum. Experiments were performed using sex- and age-matched controls. Animals were handled according to protocols approved by the Weizmann Institute Animal Care Committee (IACUC) as per international guidelines.

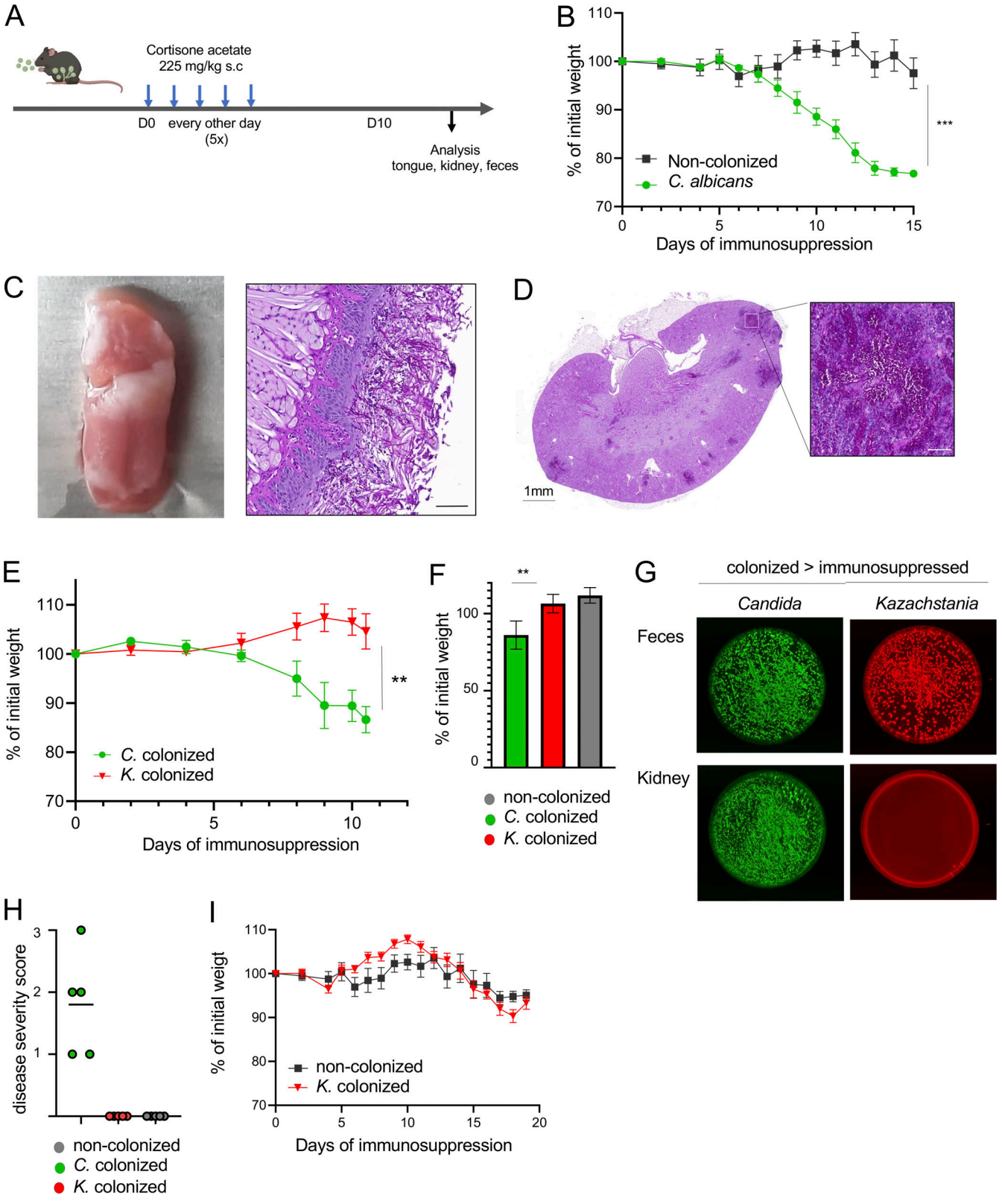

Figure 5. **Commensal *C. albicans* but not *K. weizmannii* cause pathology in immunosuppressed animals. (A)** Schematic of the experimental setup for immunosuppression protocol. **(B)** Weight curve of *C. albicans*–colonized mice and uncolonized controls upon cortisone 21-acetate injections; *n* = 5 mice per group, three independent experiments, error bar represents SEM. The corresponding statistical analysis used two-tailed Student's *t* test, comparing differences of groups in the last time point of experiment. **(C)** Representative pictures of tongue candidiasis observed in *C. albicans*–colonized mice day 10 after immunosuppression, PAS staining. Scale bars represent 50 µm. **(D)** Representative picture of *C. albicans*–induced kidney pathology, PAS staining. Scale bars represent 50 µm. **(E)** Weight loss curve, comparison of *C. albicans* and *K. weizmannii* colonized mice, *n* = 4–8 mice per group, four independent experiments,

error bar represents SEM. The corresponding statistical analysis used two-tailed Student's *t* test, comparing differences of groups in the last time point of experiment. **(F)** Percent of initial weight in the endpoint of the experiment; graph represents mean with SEM. The corresponding statistical analysis used two-tailed Student's *t* test, comparing differences of groups in the last time point of experiment. **(G)** Representative picture of *C. albicans* and *K. weizmannii* recoverable by plating of feces (10 ng) and kidneys (10 mg) of *C. albicans*– or *K. weizmannii*–colonized animals (with Abx) 10 days after immunosuppression. **(H)** Pathology score based on microscopic and macroscopic evaluation of kidneys. **(I)** Weight loss comparison between *K. weizmannii*– and non-colonized animals. n = 5 per group, three independent experiments, error bar represents SEM. ** P ≤ 0.01, *** P ≤ 0.001.

Microbes

The recombinant *C. albicans* SC5314 strain expressing ENO1-GFP fusion protein was obtained from J. Berman (Tel Aviv University, Tel Aviv, Israel) (Gonia et al., 2017). *K. weizmannii* was first cultivated from the feces of mice housed in the Weizmann Institute SPF facility. The fluorescent *K. weizmannii* strain with a fusion of ENO1 to the modified miRFP 670 (herein Kazachstania-miRFP) was generated using CRISPR/Cas9 targeted mutagenesis (Gonia et al., 2017). Insertion in ENO1 locus was confirmed using genomic PCR with primers ENO F (5′-CGGTCAAATCAAGAC TGGTGCTC-3′) and miRFP Nano R1 (5′-GCTGTTGCTGTTGCT GTAAAAGA-3′) or Mirf R Screen (5′-CTACCATGGGAGTATTCT TCTTCACC-3′). *C. albicans* strains were cultured on solid YPD media at 30°C for 24–36 h. *K. weizmannii* and Kazachstania-miRFP were cultured on solid YPD media at 37°C. *K. heterogenica* Y-27499 was obtained from the ARS Culture Collection (https://nrrl.ncaur.usda.gov/) and cultured on solid YPD media at 37°C for 24 h. *C. parapsilosis* (5′-ATCC-3′, 2001) and *C. glabrata* were cultured on solid YPD media at 30°C for 24 h.

Fungal gut colonization

To establish intestinal colonization with *C. albicans* and *K. weizmannii*, the drinking water of mice was supplemented with ampicillin (1 mg/ml, ampicillin sodium salt 5 G cat. 9518; Sigma-Aldrich) 2–3 days prior to oral fungal inoculation. Mice were maintained on Abx-supplemented drinking water throughout the whole experiment unless stated otherwise. For oral inoculation, *C. albicans* and *K. weizmannii* were grown on solid YPD media at 30°C or 37°C, respectively. Cultures were washed with PBS, and 10^7 yeast cells in 30 µl PBS were administered dropwise into the mouths of mice. For the inoculation of mixed cultures, a culture of 10^7 cells of each species was used. Non-colonized mice kept on ampicillin-supplemented water were used as the control.

Immunosuppression

Stably fungal-colonized mice were 5x s.c injected with 225 mg kg^{-1} with cortisone 21-acetate (C3130; Sigma-Aldrich), following the scheme of injection every other day as described previously (Solis and Filler, 2012). Mice were monitored for weight loss. Following sacrifice, the organs and feces were collected for histological examination, flow cytometry, and fungal cultivations. If the weight dropped to 20% of the starting weight, mice were sacrificed according to IACUC protocol.

Determination of colony-forming units (CFU)/g tissue/feces

For enumerating the number of recoverable *C. albicans* and *K. weizmannii* CFU, individual fecal pellets or each tissue from mice was sterilely dissected, weighed, and homogenized in sterile double-distilled water (DDW). Serial dilutions on the organ homogenate were spread onto YPD media plates and the number of individual colonies enumerated after incubation at 37°C for 24 h. Plates were imaged by Bio-Rad ChemiDoc MP Imaging system.

Genomic PCR for yeast identification and quantification

Adopting a reported protocol (Dobeš et al., 2022), 25 mg of feces or tissue were surgically resected including its content. Samples were treated with Proteinase K and then homogenized using Lysing Matrix C (MP Biomedicals) with the Omni Bead Ruptor 24 (Omni International, Inc.). DNA was extracted using Quick-DNA plus kit (Zymo Research) according to the manufacturer's instructions. 10 ng of isolated DNA was used for quantitative PCR reaction using Fast SYBR green Master Mix (cat. 4385614; Thermo Fisher Scientific). Reaction was performed on the Quantstudio 7 Flex Real-Time PCR system (Thermo Fisher Scientific) using the fast SYBR 10 µl program. Fungal DNA content in the samples was calculated using standard curves with known DNA concentration from cultured fungi and normalized to tissue weight and number of amplicons. For detection of *C. albicans*, we used previously published primers (He et al., 2020). For identification of fungi in colonized animals, feces were plated on YPD, following DNA purification from single colony and ITS1 detection via PCR reaction. PCR products were sequenced using in-house Sanger sequencing. Primer sequences are listed in Table 1.

Fecal DNA extraction for 16S rRNA gene sequencing

DNeasy Blood and Tissue Kit (cat. 69504) was used according to the manufacturer's instructions for fecal DNA isolation for 16S sequencing. Prior to the kit isolation, frozen fecal samples were digested with proteinase K in ALT buffer of the kit at 56°C, followed by bead-beating with sterile zirconia beads (0.1 mm diameter, cat. no. 11079101; BioSpec)

16S rRNA gene sequencing and taxonomic assignment

PCR amplification of fecal DNA was performed by Hylabs Company using PCRbio Hot start ready mix using 2 µl of DNA and custom primers covering the V4 region primers from Earth Microbiome Project (CS1_515F [V4_F], 5′-ACACTGACGACAT GGTTCTACAGTGCCAGCMGCCGCGGT-3′ and CS2_806R [V4_R], 5′-TACGGTAGCAGAGACTTGGTCTGGACTACHVGGGTWTCT-3′) for 25 cycles in a volume of 25 µl. Of the reaction, 2 µl was used for a second PCR amplification of 10 cycles in 10 µl using Fluidigm Access Array Barcode library according to the manufacturer's protocol (2 µl barcode per reaction). DNA was purified using Kapa Pure Beads at a ratio of 0.65× and quantified with Qubit fluorometer using Denovix dsDNA high sensitivity assay. DNA size and integrity was quantified by Agilent TapeStation DNA ScreenTape. Samples were sequenced on MiSeq (Illumina) machine with 30% PhiX using MiSeq Reagent Kit v2 500PE.

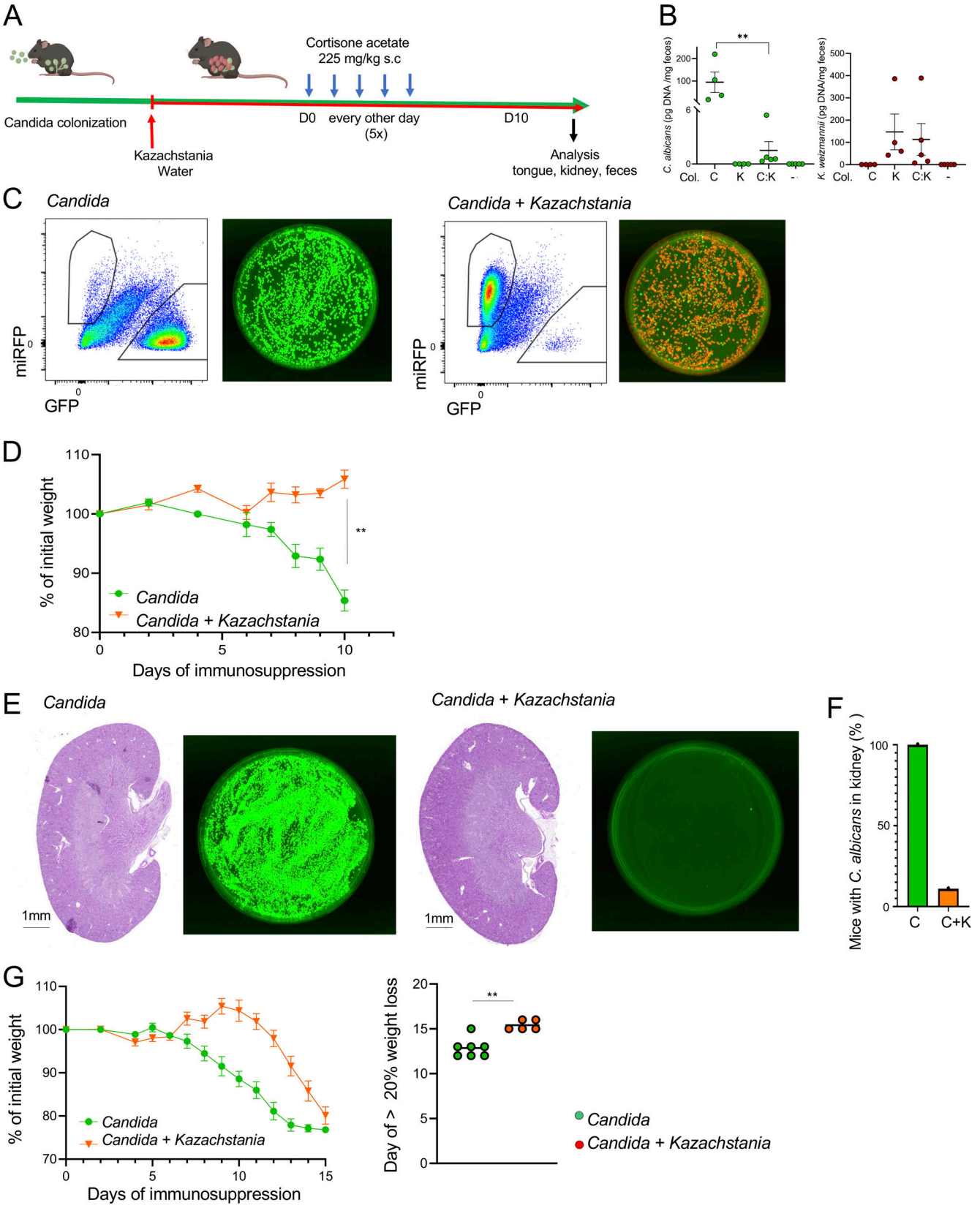

Figure 6. ***K. weizmannii* mitigates *C. albicans*–induced pathology in immunosuppressed mice. (A)** Schematic of immunosuppression protocol of *C. albicans*–colonized mice and oral *K. weizmannii* exposure. **(B)** Quantitative PCR analysis of genomic DNA of *C. albicans* and *K. weizmannii*, analyzed following 10 days of immunosuppression. Data shown as mean ± SEM; statistical significance calculated using ANOVA, $P < 0.05$; $N = 4–5$ per group. **(C)** Representative picture of recoverable *C. albicans* and *K. weizmannii* from feces of *C. albicans*–colonized animals with or without *K. weizmannii* supplementation in their drinking

water, analyzed by flow cytometry and cultivation 10 days after the first cortisone-acetate injection. **(D)** Weight monitoring curve (% initial weight), comparison of immunosuppressed animals following *C. albicans* colonization and *K. weizmannii*–outcompeted *C. albicans* colonization. All mice were sacrificed 10 days after the first dose of cortisone-acetate injection. The corresponding statistical analysis used two-tailed Student's *t* test, comparing the differences of groups in the last time point of experiment. **(E)** Representative picture of kidneys (PAS staining) of immunosuppressed animals following *C. albicans* colonization and *K. weizmannii*–outcompeted *C. albicans* colonization and results of cultivations of 1 mg kidney homogenate. Kidneys were analyzed 10 days after the first cortisone-acetate injection. **(F)** Bar graph indicating percentage of mice displaying *C. albicans* dissemination to kidneys as detected by plating and conformed by histology. *C. albicans* and *C. albicans*/*K. weizmannii*–outcompeted animals ($N = 9$ per group). **(G)** Weight monitoring curve (% initial weight): *C. albicans* and *K. weizmannii*–outcompeted animals; error bar represents SEM, comparison of the day reaching >20% weight loss. The corresponding statistical analysis used two-tailed Student's *t* test, comparing differences of groups in the last time point of the experiment. ** $P \leq 0.01$.

Demultiplexing was performed using bcl2fastq with default parameters allowing for 0 mismatches. Data were then mapped to PhiX using bowtie2 to remove PhiX control and unmapped reads were quantified, collected, and examined using fastQC. Demultiplexed reads were uploaded into CLC genomics workbench (Qiagen) and analyzed using their 16S microbiome pipeline. The analysis workflow consisting of quality filtration of the sequence data, and operational taxonomic unit (OTU) clustering was performed with default parameter settings. The adaptor sequence was removed and the reads with a quality score <25 or length <150 were discarded. The maximum number of acceptable ambiguous nucleotides was set to 2 and the length of the reads was fixed at 200–500 bp. Chimeric sequences and singletons were detected and discarded. The remaining unique reads were used for OTU clustering, which was performed by alignment to the SILVA database at 97% sequence similarity.

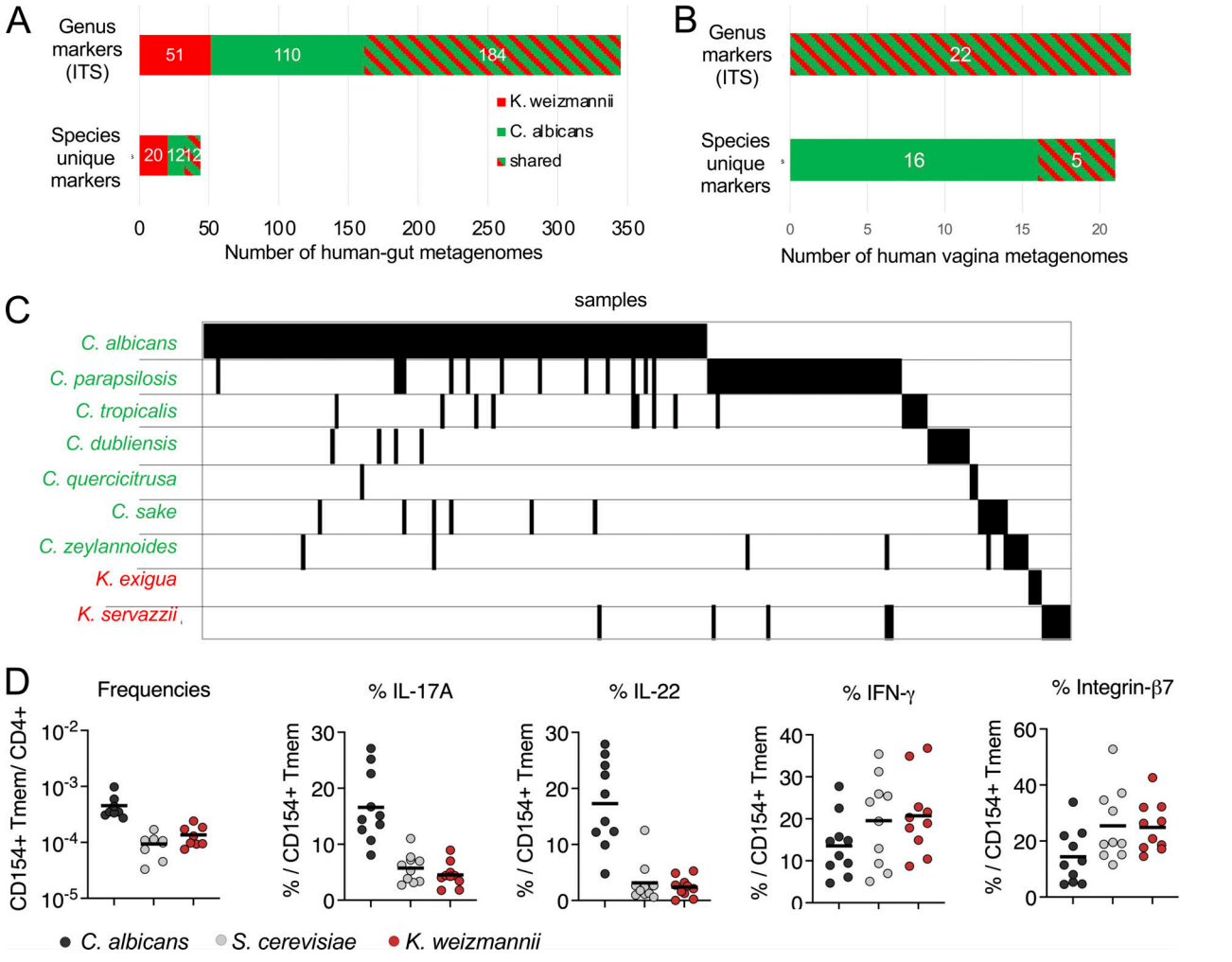

Figure 7. ***Kazachstania* presence in human metagenomes. (A)** Number of human gut metagenomes that were identified for either *C. albicans* (green), *K. weizmannii* (red), or both (mixed color), using genus-level markers (top) or using unique species-level markers (bottom). Numbers are out of 7,059 examined metagenomic datasets. **(B)** Number of human vagina metagenomes that were identified for either *C. albicans* (green), *K. weizmannii* (red), or both (mixed color), using genus-level markers (top) or using unique species-level markers (bottom). Numbers are out of 173 metagenomic datasets. **(C)** ITS2 analysis of fecal samples of a cohort of 570 healthy individuals for the presence of *Candida* and *Kazachstania* spp. **(D)** ARTE analysis of anti-fungal CD4⁺ T cell reactivity in the blood of human individuals ($n = 10$).

Table 1. **Genomic PCR for yeast identification and quantification**

Yeast strain	Forward primer (5′-3′)	Reverse primer (5′-3′)
C. albicans	GGTGTTGAGCAATACGAC	AGACCTAAGCCATTGTC
C. parapsilosis	GGTTGATTACATGCGCGATCT	GGACGATAAACCCTACCA GCG
C. glabrata	CCAGAAGATCTTGAACCAACT GC	GTTGTGGCATGATGAGTG ACC
K. weizmannii *K. heterogenica*	ATGCACGTTTTTCTGGGTGC	GTATCGCATTTCGCTGCGTT

Bioinformatics analysis of 16S rRNA gene sequencing data

Visualization of OTU counts was done using the Marker Data profiling pipeline of MicrobiomeAnalyst (Chong et al., 2020). Counts were filtered to include OTUs with minimum two counts (mean abundance value) and scaled to library total sum. Abundance profiles were generated after merging small taxa with counts <10 based on their median counts. To explore uncultured species (D6 level), the annotations of "uncultured bacteria" were concatenated to their family names (D4 level). Results were used for Alpha diversity analysis using Shannon diversity, *T* test on filtered data, and Beta Diversity (PCoA using Bray-Curtis index) plots.

Bioinformatics screening of human shotgun metagenomics datasets to identify fungi species

Identification of genomic regions unique to K. weizmannii *and* C. albicans

To identify *K. weizmannii* and *C. albicans* in human metagenomics datasets, we first selected a set of nucleotide regions that are unique to the genome sequence of either *K. weizmannii* or *C. albicans* and used them to specifically identify these fungi in the background of other fungi, bacteria, and other species in the metagenomes. The genome assemblies of *K. weizmannii* and *C. albicans* were compared with 22 genomes (genus *Kazachstania*) and 11 genomes (genus *Candida*), respectively (Tables S1, S2, S3, and S4), using the GView Server (Petkau et al., 2010), with analysis type "Unique genome" with default parameters except for the Genetic code, where "Standard" was used. Nucleotide regions unique to each target genome were collected and further compared with the NCBI nt database using BLAST (E-value <0.0001) to exclude regions that are also present in bacteria or other nonfungal organisms. This search resulted in 179 nucleotide sequences specific to *K. weizmannii* and 904 nucleotide sequences specific to *C. albicans*.

Screening shotgun metagenomics datasets using unique Kazachstania *sp. and* C. albicans *queries*

A dataset of 13,174 metagenomes, collected from the Global Microbial Gene Catalog v1.0 (GMGC; Coelho et al., 2022), was screened to identify sequences that originate from either *Kazachstania* sp. or *C. albicans* genomes. Each GMGC metagenome was originally stratified into habitats, and its raw nucleotide sequences were assembled into thousands of contigs (provided to us by Luis Pedro Coelho, Queensland University of Technology, Brisbane, Queensland, Australia). All assembled contigs from each metagenomics sample were used as a query and were searched against the set of unique *K. weizmannii* or *C. albicans* sequences constructed as described above as a reference. Alignments were generated using bowtie2 algorithm (version 2.3.5.1, using --local mode). To broaden the search to genus level, all metagenomics assemblies were also mapped to a set of genus-specific rRNA and ITS sequences, extracted from *K. weizmannii* or *C. albicans* genomes (namely 25Sa, 18Sa, 5.8Sa, ITS1a, ITS2a, ETS1a, ETS2a). To avoid biases in the specificity of ITS searches, we counted only sequences which mapped to ITS regions without mutations (using the "XM:i:0" tag in the alignment file).

Genomic DNA isolation from fungal cultures

Fungal pellet was dissolved in 2 ml lysis buffer (100 mM Tris pH 8.0, 50 mM EDTA, 1% SDS) and sonicated for 10 s. 300 µl of the supernatant was transferred to 300 µl 7 M ammonium acetate pH 7.0, vortexed, and incubated for 5 min at 65°C followed by 3 min on ice. 500 µl chloroform was added and the solution was mixed by inverting the tube. Samples were spun for 10 min at 13,000 rpm at 4°C. 300 µl of the upper phase was transferred to 400-µl isopropanol-filled tubes and incubated for 5 min on ice. Samples were spun for 10 min at 13,000 rpm at 4°C and the pellet was washed with 800 µl 70% EtOH, spun for 1 min at maximum speed, air dried, and dissolved in DDW.

Genome sequencing, annotation, and comparison

Sequencing and hybrid (Nanopore and Illumina) assembly were performed by SeqCenter, as follows: Illumina—Sample libraries were prepared using an Illumina DNA Prep kit and IDT 10 bp UDI indices and sequenced on an Illumina NextSeq 2000 producing 2 × 151 bp reads. The data were demultiplexed and adapters removed using bcl2fastq [2] (v2.20.0.445) (https://support.illumina.com/sequencing/sequencing_software/bcl2fastq-conversion-software.html). Nanopore—Samples were prepared for sequencing using Oxford Nanopore's "Genomic DNA by Ligation" kit (SQK-LSK109) and protocol. All samples were run on Nanopore R9 flow cells (R9.4.1) on a MinION. Basecalling was performed with Guppy (version 4.2.2) in high-accuracy mode (default parameters + effbaf8). Quality control and adapter trimming was performed with porechop (https://github.com/rrwick/Porechop) version 0.2.2_seqan2.1.1 with the default parameters. Long-read assembly with Oxford Nanopore Technology reads was performed with flye (version 2.8) (Grant et al., 2012). The long read assembly was polished with pilon (1.23) (Walker et al., 2014). Annotation was performed with the Yeast Gene Annotation Pipeline (YGAP) (Proux-Wéra et al., 2012) with the post-WGD settings, and Companion for Fungi (Steinbiss et al., 2016) with a reference organism of *C. glabrata* CBS138. The output of both programs was compared with CD-HIT (version 4.8.1) with c = 1 to reduce redundancy, and the remaining genes were combined with YGAP as the base annotation using in-house scripts. Whole genome comparison of 27 species of *Kazachstania* on the basis of *K. weizmannii* was performed with CCT (CGView Comparison Tool) (Grant et al., 2012), with a BlastN e-value of e–10.

Phylogenetic analysis

The d1d2 region of 26SrDNA of various species (Table S1) were aligned with both ClustalW2.1 (Larkin et al., 2007) and Muscle 3.8.31 (Edgar, 2004). Phylogenetic trees were constructed with Maximum likelihood and DNA parsimony using PhyML 3.0 (Guindon et al., 2010), DNAML, DNAPARS, and DNAPENNY in the Phylip package (3.697) developed by Felsenstein. The Phylip trees were then processed through Consense. Trees with similar topologies were obtained, and the Muscle/DNAPENNY tree is shown. The tree was visualized with iTol version 6 (Letunic and Bork, 2021).

In vitro serum antibody binding assay

Adopting a reported protocol (Ost et al., 2021), briefly, blood was collected from mice and rested at room temperature (RT) for 1 h, followed by centrifugation at 2,000 *g* for 10 min. Serum supernatant was collected and frozen at −80°C until use. Cultured fungi were normalized to OD_{600} = 1 in PBS supplemented with 1% bovine serum albumin and 0.01% sodium azide (PBA solution). Cultured fungi were incubated with 20× diluted mouse serum on ice for 45 min, then washed twice with PBA, followed by staining with anti-mouse IgA and IgG. Samples were recorded on Cytek Aurora and analyzed in FlowJo (Tree Star). Antibody binding intensity was normalized to the negative controls. Isotype control, non-stained and no-serum were used as negative controls.

Tissue isolation for flow cytometry

Mesenteric and peripheral lymph nodes were aseptically resected out into sterile, ice-cold PBS and mashed manually using a 1-ml syringe plunger through a 80-µm nylon cell strainer. 100–200 µl of mouse blood was collected from submandibular vein, resuspended in 15 µl of heparin (Sigma-Aldrich) to prevent coagulation, followed by lysis with 1 ml ACK buffer (8.29 g/ml NH_4Cl, and 1 g/liter $KHCO_3$, 37.2 mg/liter Na-EDTA) for 5 min RT and subsequent centrifugation.

Cell staining, stimulation, and flow cytometry and microscopy

Methods adhered to published guidelines (Cossarizza et al., 2019). For cytokine staining, cells were incubated for 3 h with Cell Activation Cocktail (with brefeldin A) (423303; BioLegend) in10% FBS in RPMI at 37°C, followed by extracellular marker staining. Intracellular Fixation and Permeabilization Buffer Set (Invitrogen) was used according to the manufacturer's instruction. For transcription factor staining, Foxp3/Transcription Factor Staining Buffer Set (Invitrogen) was used according to the manufacturer's instruction. Flow cytometry samples were recorded on BD LSR Fortessa 4 lasers or Cytek Aurora followed by data analysis using the FlowJo software (Tree Star).

Histology

Mice were euthanized, and intestines, kidneys, and tongue were excised and fixed overnight in 4% paraformaldehyde (PFA) at 4°C. Paraffin embedding and sectioning were performed by the institutional histology unit. For histopathology of typical tongue or kidney fungal lesions in the mouse model of immunosuppression, paraffin sections were stained with periodic acid-Schiff (PAS) or H&E and slides were captured using a Panoramic SCAN II (3DHISTECH) and analyzed using CaseViewer software (3DHISTECH). Reagents and resources are listed in Table 2.

Table 2. **Reagents and resources used in this study**

Reagent or resource	Source	Identifier
IgA, PE	Invitrogen	Cat#12-4204-81
IgG, Alexa Fluor 594	BioLegend	Cat#405326
CD45, Violet 450	Biogems	Cat#07512-40-108
CD4, Alexa Fluor 647	BioLegend	Cat#100412
TCR β chain, FITC	BioLegend	Cat#109206
IgG1 κ Isotype Ctrl, PE	BioLegend	Cat#400407
ROR gamma (t)	Invitrogen	Cat#12-69981-80
IFNg, APC	BioLegend	Cat#505810
IL17, PE	BioLegend	Cat#506904
TCR β chain, PE/Cyanine5	BioLegend	Cat#109209
CD274, PE/Dazzle 594	BioLegend	Cat#124323
CD43, Alexa Fluor 700	BioLegend	Cat#143214
Ly6C, Pacific Blue	BioLegend	Cat#128014
Ly6G, FITC	BioLegend	Cat#127605
CD115, APC/Cyanine7	BioLegend	Cat#135532
CD11b, PE	BioLegend	Cat#101207
CD220, APC	BioLegend	Cat#103212
Zombie Aqua Fixable Viability Kit	BioLegend	Cat#423102
purified CD16/32	BioLegend	Cat#101302
Cell Activation Cocktail	BioLegend	Cat#423302
Brefeldin A Solution	BioLegend	Cat#420601
Fixation/Permeablization Kit	BD Bioscience	Cat# 554714
True-Nuclear TF Buffer Set	BioLegend	Cat#424401

ARTE

Peripheral blood mononuclear cells (PBMCs) were freshly isolated from EDTA blood samples on the day of blood donation by density gradient centrifugation (Biocoll; Biochrom). ARTE was performed as previously described (Bacher et al., 2013, 2019). In brief, 2 × 10e7 PBMCs were plated in RPMI-1640 medium (GIBCO), supplemented with 5% (vol/vol) human AB-serum (Sigma-Aldrich) at a cell density of 1 × 10e7 PBMCs/2 cm^2 in cell culture plates and stimulated with 40 µg/ml fungal lysates for 7 h in presence of 1 µg/ml CD40 and 1 µg/ml CD28 pure antibody (both Miltenyi Biotec). 1 µg/ml brefeldin A (Sigma-Aldrich) was added for the last 2 h. Cells were labeled with CD154-biotin followed by anti-biotin MicroBeads (CD154 MicroBead Kit; Miltenyi Biotec) and magnetically enriched by two sequential MS columns (Miltenyi Biotec). Surface staining was performed on the first column, followed by fixation, permeabilization (Inside Stain Kit; Miltenyi Biotec), and intracellular staining on the second column. The following antibodies

were used: CD4-APC-Vio770 (M-T466), CD8-VioGreen (REA734), CD14-VioGreen (REA599), CD20-VioGreen (LT20), Integrin-b7-PE-Vio770 (REA441) (all Miltenyi Biotec); CD45RA-PE-Cy5 (HI100), IFN-γ-BV785 (clone: 4S.B3) (both Biolegend); IL-17A-BV650 (clone: N49-653), IL-22-PerCP-eFluor710 (clone: IL22JOP) (both BD Biosciences). Viobility 405/520 Fixable Dye (Miltenyi Biotec) was used to exclude dead cells. Data were acquired on an LSR Fortessa (BD Bioscience).

Frequencies of antigen-specific T cells were determined based on the total cell count of $CD154^+$ T cells after enrichment and normalized to the total number of $CD4^+$ T cells applied on the column. For each simulation, background cells enriched from the non-stimulated control were subtracted.

ITS2 amplification and sequencing of human stool samples

Human stool samples analyzed in this study were collected as part of a previous study, approved by Tel Aviv Sourasky Medical Center Institutional Review Board (IRB), the Kfar Shaul Hospital IRB, and the Weizmann Institute of Science Bioethics and Embryonic Stem Cell Research oversight committee (for details see Zeevi et al., 2015). ITS2 sequencing was used for fungal identification as described in Narunsky-Haziza et al. (2022). Briefly, ITS2 sequencing was applied to 570 human stool samples and 6 controls (Korem et al., 2017; Zeevi et al., 2015). PCR was performed on 10 ng of DNA per sample (or the maximum available). Three PCR batches were required with two wells left empty as library controls in each batch. Forward primer ITS86F 5′-759 GTGAATCATCGAATCTTTGAA-3′ and reverse primer ITS4 with rd2 Illumina adaptor 5′-AGACGTGTGCTCTTCCGATCT-TCCTCC GCTTATTGATATGC-3′ were used for the first PCR amplification. PCR mix per sample contained 5 µl sample DNA, 0.2 µM per primer (primers purchased from Sigma-Aldrich), 0.02 U/µl of Phusion Hot Start II DNA Polymerase (763 F549; Thermo Fisher Scientific), 10 µl of X5 Phusion HS HF buffer, 0.2 mM dNTPs (Larova GmbH), 31.5 µl ultrapure water, for a total reaction volume of 50 µl. PCR conditions used were 98°C for 2 min, (98°C for 10 s, 55°C for 15 s, 72°C for 35 s) X 30, 72°C for 5 min. A second PCR was performed to attach Illumina adaptors and barcode per sample for six additional cycles. Samples from the first PCR were diluted 10-fold and added to the PCR mix as described above. Primers of second PCR included forward primer P5-rd1-768 ITS86F 5′-AATGATACGGCGACCACCGAGATCTAC ACTCTTTCCCTACACGACGCTCTTCCGATCT-GTGAATCATCGA ATCTTTGAA-3′, and reverse primer 5′- CAAGCAGAAGACGGC ATACGAGAT-NNNNNNNN-GTGACTGGAGTTCAGACGTGTGCT CTTCCGATCT-3’. Every 96 samples were combined for a single mix by adding 14 µl from each. Before mixing, an aliquot from each of the samples was run on an agarose gel. In cases where the amplified bands were very strong, samples were diluted between 5- and 20-fold before they were added to the mix. Each sample mix was cleaned with QIAquick PCR purification kit (catalog # 28104; Qiagen). Two cleaned sample mixes were then combined into a single mix of 192 samples and size selection was performed with Agencourt AMPure XP beads (#A63881; Beckman Coulter) to remove any excess primers. Beads to sample ratio was 0.85 to 1. Samples were then run in three libraries on the Miseq v3 600 cycle paired-end with 30% PhiX.

ITS2 sequencing analysis

The ITS2 classification pipeline was built with Python 3.6. For each sequencing library, paired-end reads were joined using PEAR (version 0.9.10) followed by filtering of merged reads by a minimum length of 80 bp and trimming of primers from both ends with cutadapt (version 1.17). Within the QIIME 2 environment (version 2018.8), Dada2 was used to create amplicon sequence variants (ASVs), and then ITSx (version 1.1b1) was used to delineate ASVs to ITS2 regions (removing preceding 5.8S and trailing 28S sequences). A taxonomic naive Bayesian classifier in QIIME 2 (Bolyen et al., 2019) was trained on the UNITE database (version 8, dynamic, sh_taxonomy_qiime_ver8_dynamic_ 04.02.2020.txt) and used to classify the 180 processed ASVs. 91% of raw reads were classified to species level (Table S7). Most of the downstream analysis and plots were performed with R version 4.1.1 and phyloseq 1.34.0. ASVs were filtered by the ITSx and UNITE classifications to include fungal reads only. 119 ASVs that were classified by ITSx as fungi were included in the downstream analysis, representing over 97.5% of reads. Out of the remaining 61 ASVs that were classified by ITSx as non-fungal (Tracheophyta [T] land plants), one (fid65) was included in the downstream analysis since its classification as fungi reached all the way to species level by UNITE and was validated by NCBI BLAST to be fungal. The histogram of the number of reads per ASV per sample presented a bimodal distribution with the peaks found on either side of 100 reads/ASV or 100 reads/sample. We therefore floored the data in a sample-specific manner such that if an ASV was assigned <100 reads in a specific sample, its assigned reads were converted to zero. Next, we introduced two types of data normalization: (1) Library normalization, where samples were normalized to account for the difference in the average number of reads/sample per library. (2) Dilution normalization: ASV reads were multiplied by the dilution factor per sample to reflect their true original load. Next, ASVs were aggregated based on UNITE classification, to the species level when possible. ASVs that could not be classified to species level were grouped together by the lowest known phylogenetic level and labeled “other.” A total of 55 species were detected, 13 of which were also detected in control samples, but with a maximum of 100 reads per sample demonstrating a very mild read leakage of the higher abundant species in the library, e.g., *S. cerevisiae*. Therefore, flooring of species with <100 reads per sample was applied. Lastly, data were aggregated by summing all reads in each taxonomic level by the associated taxa in the level above it.

Strains and culturing conditions

C. albicans SC5314, *S. cerevisiae* S288C, and *K. weizmannii* were regularly cultured in YPD (1% yeast extract, 2% peptone, 2% glucose) medium or on agar plates at 30°C or 37°C. Precultures were prepared in liquid YPD and incubated at 30°C with shaking until stationary (~22 h). For growth experiments, cultures were washed twice with PBS, and adjusted to an experiment-specific OD in PBS. Where indicated, synthetic defined medium was used (SD; 6.7 g yeast nitrogen base + ammonium sulfate (Formedium), 20 g glucose, with or without 0.79 g complete supplement mixture (CSM) (Formedium) in 1 liter of distilled water).

Growth in different media and temperatures

Growth was measured in 96-well format in these media: YPD (1% yeast extract, 2% peptone, and 2% glucose), brain heart infusion (Roth), SD (Formedium) with 2% glucose ± CSM, DMEM (Dulbecco's Modified Eagle Medium; Gibco; Thermo Fisher Scientific), or RPMI 1640 (Gibco; Thermo Fisher Scientific). The initial OD was set to 0.1 using 200 µl as the total volume of media per well. Cell-free medium served as control. Each experiment was done in three biological replicates per strain and per media. The 96-well plates were incubated at either 30, 37, or 42°C, and growth was measured optically at 600 nm in a BioTek LogPhase 600 multiplate reader (Agilent Technologies, Inc.) every 10 min for 24 h. The mean growth of the replicates was visualized by R version 4.2.2 (https://www.R-project.org/).

Virulence of *K. weizmannii*

Host cell damage was determined with C2BBe1 human intestinal ECs (ATCC CRL-2102) by release of cytoplasmic LDH. The intestinal cells were seeded on collagen I–coated (10 µg/ml, 2 h at RT; Thermo Fisher Scientific) 96-well plates at a total cell density of 1×10^5 cells/ml in 200 µl DMEM, supplemented with 10% FBS (Bio & Sell), 10 µg/ml Holotransferrin (Calbiochem; Merck), and 1% non-essential amino acids (Gibco; Thermo Fisher Scientific), and then incubated for 48 h at 37°C and 5% CO_2.

Overnight yeast cultures were semi-synchronized by diluting in YPD to an OD of 0.2, followed by 4 h at 30°C, 180 rpm shaking. The precultures each were then washed twice with 1 ml sterile PBS, dissolved in 1 ml DMEM, and adjusted to 8×10^5 cells/ml in DMEM singly or as coinfection. The medium was removed from the C2BBe1 cells by aspiration, and 100 µl DMEM without FBS and 100 µl of the yeast suspensions (or DMEM alone) were added in technical triplicates. The cells were incubated for 24 h at 37°C with 5% CO_2. Host cell damage was detected with the Cytotoxicity Detection Kit (Roche) from the supernatants according to the manufacturer's instructions and calibrated by LDH from rabbit muscle (5 mg/ml; Roche). Data analysis was done with GraphPad Prism.

Phenotypic screening

The Phenotype MicroArrays for the microbial cells (PM) system (Biolog Inc.) was used according to the manufacturer's instructions. Colonies were transferred with sterile cotton swaps into 15 ml of sterile dH_2O at a turbidimeter transmittance of 62%. PM plates used were carbon sources (PM1-2), nitrogen sources (PM3, PM6-8), pH (PM10), and chemical inhibitors (PM21-25). Data S1 lists all tested substances. For carbon and nitrogen sources, the medium contained inoculating fluid IFY-0 base, redox dye mix D (Biolog Inc.), potassium phosphate, and sodium sulfate, supplemented with L-glutamic acid monosodium (for PM1-2) or glucose (for PM3, PM6-8) (Sigma-Aldrich). For inhibitors and pH (PM10, PM21-25), SD medium (Formedium) supplemented with CSM (Formedium), redox dye mix E (Biolog Inc.), ammonium sulfate, and glucose were used. Metabolic activity of 100 µl yeasts suspension was followed as a color reaction over 48 h at 37°C every 15 min in biological triplicates. Data were processed using Biolog Data Analysis 1.7 (Biolog Inc.) and analyzed by a previously described R pipeline (Vehkala et al., 2015) and the package opm version 1.3.77 (Vaas et al., 2013) to group into active log growth and non-active, and calculate the area under the curve (AUC). AUCs were normalized for each species to growth with either glucose (for carbon sources), glutamine (nitrogen sources), or inhibitor-free test medium at the same pH of 5 (inhibitors). The difference between the normalized AUCs of *C. albicans* and *K. weizmannii* (Difference = AUC(*K. weizmannii*) − AUC(*C. albicans*)) was used to calculate the z-scores ($z - score = \frac{Difference - Mean(Difference)}{SD(Difference)}$). Substances with z-scores >2 or less than −2 were graphed with ggplot2 (https://ggplot2.tidyverse.org).

Filamentation assay

C. albicans and *K. weizmannii* were tested for their ability to the filament in liquid filamentation conditions. Yeast cells were grown overnight in liquid YPD at 30°C or 37°C, respectively, were centrifuged and washed 2× with PBS prior to the experiment, and the strains were diluted on the same OD. Yeast cells were incubated for 5 h at 30, 37, or 42°C with shaking, then directly fixed with 4% PFA in PBS for 30 min, followed by washing with PBS, and images were captured by bright Zeiss field microscope.

In all experiments, data are presented as the mean ± SEM unless stated otherwise. Statistical significance was defined as $P < 0.05$. The number of animals is indicated as *n*. Animals of the same age, sex, and genetic background were randomly assigned to treatment groups.

Online supplemental material

Fig. S1 is related to Fig. 1, showing the data related to the PCR-based ITS1 region analysis and the cultures under distinct temperatures and media shown in Fig. 2 F, as well as Fig. 2 G. Fig. S2 is related to the generation of *K. weizmannii* reporter strain (Fig. S2, A and B) and gives examples for the flow cytometric analysis of the fecal samples related to Fig. 3 L. Fig. S3 is related to the microbiome analysis (Fig. S3, A–C), the colonization of germ-free and Abx-treated animals (Fig. 3 M) (Fig. S3, C–F), and the serum antibody titer analysis (Fig. 4 C) (Fig. S3, G and H). Fig. S4 is related to the immunosuppression experiment shown in Fig. 5. Data S1, S2, and S3 are related to the Biolog analysis, the cultures under distinct temperatures and media shown in Fig. 2 F, and the EC coculture assay (Fig. 4 G), respectively. The supplemental tables are related to the phylogenetic analysis (Tables S1, S2, S3, and S4), the intestinal and vaginal metagenome analysis shown in Fig. 7, A and B and Fig. S5 (Tables S5 and S6), and the analysis of the local human fecal samples shown in Fig. 7 C (Table S7).

Data availability

Sequencing data have been deposited to BioProject accession numbers PRJNA949686 and PRJNA936566 in the NCBI BioProject database (https://www.ncbi.nlm.nih.gov/bioproject/). Genomes of *K. heterogenica* and *K. weizmannii* can be found in NCBI as GCA_036320825.1 and GCA_036370985.1.

Acknowledgments

We would like to thank J. Berman (Tel Aviv University, Tel Aviv, Israel) for providing the recombinant *C. albicans* (SC5314)

reporter strain, Travis W. Adkins, (NRRL collection) for prompt yeast delivery, J. Zahradnik and G. Schreiber (Weizmann Institute, Rehovot, Israel) for the plasmid encoding the modified miRFP670 fluorescent protein, M. Lotan-Pompan and A. Weinberger for help with the bioinformatic analysis, S. Schäuble and M. Mirhakkak for providing the R script for the Biolog data analysis, C. Bar-Natan for help with the germ-free animal experiment, and L.P. Coelho for helping with access to the metagenomes.

S. Jung was funded by the Israeli Science Foundation (grant #696/21) and by the Bridge, Innovate, Nurture, Advance program of the Weizmann Institute. This research was generously supported by Morris Kahn Institute for Human Immunology. S. Jung is the incumbent of the Henry H. Drake Professorial Chair of Immunology. P.M. Jansen, S. Brunke, and B. Hube were funded by the Deutsche Forschungsgemeinschaft (DFG) through the Cluster of Excellence "Balance of the Microverse," DFG project number 390713860. P. Bacher was funded by the Cluster of Excellence EXC2167 "Precision Medicine in Chronic Inflammation," Project ID 390884018.

Author contributions: J. Sekeresova Kralova made the initial observation and conceived the project with S. Jung. C. Donic performed the yeast quantifications and serum titer analysis. S. Boura-Halfon and S. Trzebanski provided animals and helped with analysis. S. Ben-Dor and L. Fidel performed the genome analysis. B. Dassa, I. Livyatan, L. Narunsky-Haziza, O. Asraf, D. Zeevi, E. Segal, Y. Pilpel, and R. Straussman contributed the human microbiome analysis. P. Bacher performed human T cell analysis. P.M. Jansen, S. Brunke, and B. Hube performed the Biolog analysis. G. Jona helped with yeast culture. O. Brenner performed histology. H. Dafni and N. Stettner helped with the sentinel screen and germ-free analysis. N. Stettner advised on yeast biology and helped in generating the reporter strain. P. Bacher, B. Hube, S. Brunke, J.S. Kralova, and S. Jung wrote the manuscript.

Disclosures: C. Donic and S. Jung reported a patent to PCT/IL2023/050470 pending (Weizmann Institute of Science). No other disclosures were reported.

Submitted: 14 September 2023
Revised: 17 January 2024
Accepted: 14 February 2024

References

Allert, S., T.M. Förster, C.-M. Svensson, J.P. Richardson, T. Pawlik, B. Hebecker, S. Rudolphi, M. Juraschitz, M. Schaller, M. Blagojevic, et al. 2018. *Candida albicans*-induced epithelial damage mediates translocation through intestinal barriers. *MBio.* 9:e00915–e00918. https://doi.org/10.1128/mBio.00915-18

Alonso-Roman, R., A. Last, M.H. Mirhakkak, J.L. Sprague, L. Möller, P. Großmann, K. Graf, R. Gratz, S. Mogavero, S. Vylkova, et al. 2022. *Lactobacillus rhamnosus* colonisation antagonizes *Candida albicans* by forcing metabolic adaptations that compromise pathogenicity. *Nat. Commun.* 13:3192. https://doi.org/10.1038/s41467-022-30661-5

Arora, K., H. Ameur, A. Polo, R.D. Cagno, C.G. Rizzello, and M. Gobbetti. 2020. Thirty years of knowledge on sourdough fermentation: A systematic review. *Trends Food Sci. Technol.* 108:71–83. https://doi.org/10.1016/j.tifs.2020.12.008

Bacher, P., T. Hohnstein, E. Beerbaum, M. Röcker, M.G. Blango, S. Kaufmann, J. Röhmel, P. Eschenhagen, C. Grehn, K. Seidel, et al. 2019. Human anti-fungal Th17 immunity and pathology rely on cross-reactivity against *Candida albicans*. *Cell.* 176:1340–1355.e15. https://doi.org/10.1016/j.cell.2019.01.041

Bacher, P., C. Schink, J. Teutschbein, O. Kniemeyer, M. Assenmacher, A.A. Brakhage, and A. Scheffold. 2013. Antigen-reactive T cell enrichment for direct, high-resolution analysis of the human naive and memory Th cell repertoire. *J. Immunol.* 190:3967–3976. https://doi.org/10.4049/jimmunol.1202221

Basu, S., G. Hodgson, H.-H. Zhang, M. Katz, C. Quilici, and A.R. Dunn. 2000. "Emergency" granulopoiesis in G-CSF-deficient mice in response to *Candida albicans* infection. *Blood.* 95:3725–3733. https://doi.org/10.1182/blood.V95.12.3725.012k06_3725_3733

Belkaid, Y., and O.J. Harrison. 2017. Homeostatic immunity and the microbiota. *Immunity.* 46:562–576. https://doi.org/10.1016/j.immuni.2017.04.008

Bolyen, E., J.R. Rideout, M.R. Dillon, N.A. Bokulich, C.C. Abnet, G.A. Al-Ghalith, H. Alexander, E.J. Alm, M. Arumugam, F. Asnicar, et al. 2019. Reproducible, interactive, scalable and extensible microbiome data science using QIIME 2. *Nat. Biotechnol.* 37:852–857. https://doi.org/10.1038/s41587-019-0209-9

Bongomin, F., S. Gago, R.O. Oladele, and D.W. Denning. 2017. Global and multi-national prevalence of fungal diseases-estimate precision. *J. Fungi.* 3:57. https://doi.org/10.3390/jof3040057

Branco, J., I.M. Miranda, and A.G. Rodrigues. 2023. *Candida parapsilosis* virulence and antifungal resistance mechanisms: A comprehensive review of key determinants. *J. Fungi.* 9:80. https://doi.org/10.3390/jof9010080

Brown, G.D., D.W. Denning, N.A.R. Gow, S.M. Levitz, M.G. Netea, and T.C. White. 2012. Hidden killers: Human fungal infections. *Sci. Transl. Med.* 4:165rv13. https://doi.org/10.1126/scitranslmed.3004404

Chong, J., P. Liu, G. Zhou, and J. Xia. 2020. Using MicrobiomeAnalyst for comprehensive statistical, functional, and meta-analysis of microbiome data. *Nat. Protoc.* 15:799–821. https://doi.org/10.1038/s41596-019-0264-1

Coelho, L.P., R. Alves, Á.R. Del Río, P.N. Myers, C.P. Cantalapiedra, J. Giner-Lamia, T.S. Schmidt, D.R. Mende, A. Orakov, I. Letunic, et al. 2022. Towards the biogeography of prokaryotic genes. *Nature.* 601:252–256. https://doi.org/10.1038/s41586-021-04233-4

Conti, H.R., and S.L. Gaffen. 2010. Host responses to *Candida albicans*: Th17 cells and mucosal candidiasis. *Microbes Infect.* 12:518–527. https://doi.org/10.1016/j.micinf.2010.03.013

Cossarizza, A., H. Chang, A. Radbruch, A. Acs, D. Adam, S. Adam-Klages, W.W. Agace, N. Aghaeepour, M. Akdis, M. Allez, et al. 2019. Guidelines for the Use of Flow Cytometry and Cell Sorting in Immunological Studies. Second edition. Eur J Immunol, Hoboken, USA. 49:1457–1973. https://doi.org/10.1002/eji.201970107

Cypowyj, S., C. Picard, L. Maródi, J.-L. Casanova, and A. Puel. 2012. Immunity to infection in IL-17-deficient mice and humans. *Eur. J. Immunol.* 42:2246–2254. https://doi.org/10.1002/eji.201242605

Dobeš, J., O. Ben-Nun, A. Binyamin, L. Stoler-Barak, B.E. Oftedal, Y. Goldfarb, N. Kadouri, Y. Gruper, T. Givony, I. Zalayat, et al. 2022. Extrathymic expression of Aire controls the induction of effective T_H17 cell-mediated immune response to *Candida albicans*. *Nat. Immunol.* 23:1098–1108. https://doi.org/10.1038/s41590-022-01247-6

Doron, I., M. Mesko, X.V. Li, T. Kusakabe, I. Leonardi, D.G. Shaw, W.D. Fiers, W.-Y. Lin, M. Bialt-DeCelie, E. Román, et al. 2021. Mycobiota-induced IgA antibodies regulate fungal commensalism in the gut and are dysregulated in Crohn's disease. *Nat. Microbiol.* 6:1493–1504. https://doi.org/10.1038/s41564-021-00983-z

Edgar, R.C. 2004. MUSCLE: Multiple sequence alignment with high accuracy and high throughput. *Nucleic Acids Res.* 32:1792–1797. https://doi.org/10.1093/nar/gkh340

Fan, D., L.A. Coughlin, M.M. Neubauer, J. Kim, M.S. Kim, X. Zhan, T.R. Simms-Waldrip, Y. Xie, L.V. Hooper, and A.Y. Koh. 2015. Activation of HIF-1α and LL-37 by commensal bacteria inhibits *Candida albicans* colonization. *Nat. Med.* 21:808–814. https://doi.org/10.1038/nm.3871

Felk, A., M. Kretschmar, A. Albrecht, M. Schaller, S. Beinhauer, T. Nichterlein, D. Sanglard, H.C. Korting, W. Schäfer, and B. Hube. 2002. *Candida albicans* hyphal formation and the expression of the Efg1-regulated proteinases Sap4 to Sap6 are required for the invasion of parenchymal organs. *Infect. Immun.* 70:3689–3700. https://doi.org/10.1128/IAI.70.7.3689-3700.2002

Gonia, S., J. Berman, and C.A. Gale. 2017. Generation of fluorescent protein fusions in *Candida* species. *J. Vis. Exp.* 121:55333. https://doi.org/10.3791/55333

Gorfu, G., J. Rivera-Nieves, and K. Ley. 2009. Role of beta7 integrins in intestinal lymphocyte homing and retention. *Curr. Mol. Med.* 9:836–850. https://doi.org/10.2174/156652409789105525

Gow, N.A.R., F.L. van de Veerdonk, A.J.P. Brown, and M.G. Netea. 2011. *Candida albicans* morphogenesis and host defence: Discriminating invasion from colonization. *Nat. Rev. Microbiol.* 10:112–122. https://doi.org/10.1038/nrmicro2711

Graf, K., A. Last, R. Gratz, S. Allert, S. Linde, M. Westermann, M. Gröger, A.S. Mosig, M.S. Gresnigt, and B. Hube. 2019. Keeping *Candida* commensal: How lactobacilli antagonize pathogenicity of *Candida albicans* in an in vitro gut model. *Dis. Model. Mech.* 12:dmm039719. https://doi.org/10.1242/dmm.039719

Grant, J.R., A.S. Arantes, and P. Stothard. 2012. Comparing thousands of circular genomes using the CGView Comparison Tool. *BMC Genomics*. 13: 202. https://doi.org/10.1186/1471-2164-13-202

Guindon, S., J.-F. Dufayard, V. Lefort, M. Anisimova, W. Hordijk, and O. Gascuel. 2010. New algorithms and methods to estimate maximum-likelihood phylogenies: Assessing the performance of PhyML 3.0. *Syst. Biol.* 59:307–321. https://doi.org/10.1093/sysbio/syq010

Guo, C.-J., F.-Y. Chang, T.P. Wyche, K.M. Backus, T.M. Acker, M. Funabashi, M. Taketani, M.S. Donia, S. Nayfach, K.S. Pollard, et al. 2017. Discovery of reactive microbiota-derived metabolites that inhibit host proteases. *Cell*. 168:517–526.e18. https://doi.org/10.1016/j.cell.2016.12.021

He, Z.-X., H.-H. Zhao, and F.-K. Wang. 2020. PCR-detectable *Candida* DNA exists a short period in the blood of systemic candidiasis murine model. *Open Life Sci*. 15:677–682. https://doi.org/10.1515/biol-2020-0075

Hernández-Santos, N., and S.L. Gaffen. 2012. Th17 cells in immunity to *Candida albicans*. *Cell Host Microbe*. 11:425–435. https://doi.org/10.1016/j.chom.2012.04.008

Hooper, L.V., D.R. Littman, and A.J. Macpherson. 2012. Interactions between the microbiota and the immune system. 336:1268–1273. https://doi.org/10.1126/science.1223490

Huseyin, C.E., P.W. O'Toole, P.D. Cotter, and P.D. Scanlan. 2017. Forgotten fungi-the gut mycobiome in human health and disease. *FEMS Microbiol. Rev.* 41:479–511. https://doi.org/10.1093/femsre/fuw047

Iliev, I.D., and I. Leonardi. 2017. Fungal dysbiosis: Immunity and interactions at mucosal barriers. *Nat. Rev. Immunol.* 17:635–646. https://doi.org/10.1038/nri.2017.55

Jiang, T.T., T.-Y. Shao, W.X.G. Ang, J.M. Kinder, L.H. Turner, G. Pham, J. Whitt, T. Alenghat, and S.S. Way. 2017. Commensal fungi recapitulate the protective benefits of intestinal bacteria. *Cell Host Microbe*. 22: 809–816.e4. https://doi.org/10.1016/j.chom.2017.10.013

Korem, T., D. Zeevi, N. Zmora, O. Weissbrod, N. Bar, M. Lotan-Pompan, T. Avnit-Sagi, N. Kosower, G. Malka, M. Rein, et al. 2017. Bread affects clinical parameters and induces gut microbiome-associated personal glycemic responses. *Cell Metab.* 25:1243–1253.e5. https://doi.org/10.1016/j.cmet.2017.05.002

Kurtzman, C.P., C.J. Robnett, J.M. Ward, C. Brayton, P. Gorelick, and T.J. Walsh. 2005. Multigene phylogenetic analysis of pathogenic *Candida* species in the *Kazachstania* (*Arxiozyma*) *telluris* complex and description of their ascosporic states as *Kazachstania bovina* sp. nov., *K. heterogenica* sp. nov., *K. pintolopesii* sp. nov., and *K. slooffiae* sp. nov. *J. Clin. Microbiol.* 43:101–111. https://doi.org/10.1128/JCM.43.1.101-111.2005

Lallemand, Y., V. Luria, R. Haffner-Krausz, and P. Lonai. 1998. Maternally expressed PGK-Cre transgene as a tool for early and uniform activation of the Cre site-specific recombinase. *Transgenic Res.* 7:105–112. https://doi.org/10.1023/A:1008868325009

Larkin, M.A., G. Blackshields, N.P. Brown, R. Chenna, P.A. McGettigan, H. McWilliam, F. Valentin, I.M. Wallace, A. Wilm, R. Lopez, et al. 2007. Clustal W and clustal X version 2.0. *Bioinformatics*. 23:2947–2948. https://doi.org/10.1093/bioinformatics/btm404

Leonardi, I., I.H. Gao, W.-Y. Lin, M. Allen, X.V. Li, W.D. Fiers, M.B. De Celie, G.G. Putzel, R.K. Yantiss, M. Johncilla, et al. 2022. Mucosal fungi promote gut barrier function and social behavior via Type 17 immunity. *Cell*. 185:831–846.e14. https://doi.org/10.1016/j.cell.2022.01.017

Letunic, I., and P. Bork. 2021. Interactive tree of life (iTOL) v5: An online tool for phylogenetic tree display and annotation. *Nucleic Acids Res.* 49: W293–W296. https://doi.org/10.1093/nar/gkab301

Lin, J.-D., J.C. Devlin, F. Yeung, C. McCauley, J.M. Leung, Y.-H. Chen, A. Cronkite, C. Hansen, C. Drake-Dunn, K.V. Ruggles, et al. 2020. Rewilding Nod2 and Atg16l1 mutant mice uncovers genetic and environmental contributions to microbial responses and immune cell composition. *Cell Host Microbe*. 27:830–840.e4. https://doi.org/10.1016/j.chom.2020.03.001

Ling, Z., M. Zhu, X. Liu, L. Shao, Y. Cheng, X. Yan, R. Jiang, and S. Wu. 2021. Fecal fungal dysbiosis in Chinese patients with Alzheimer's disease. *Front. Cell Dev. Biol.* 8:631460. https://doi.org/10.3389/fcell.2020.631460

Martin, R., D. Albrecht-Eckardt, S. Brunke, B. Hube, K. Hünniger, and O. Kurzai. 2013. A core filamentation response network in *Candida albicans* is restricted to eight genes. *PLoS One*. 8. e58613. https://doi.org/10.1371/journal.pone.0058613

Mims, T.S., Q.A. Abdallah, J.D. Stewart, S.P. Watts, C.T. White, T.V. Rousselle, A. Gosain, A. Bajwa, J.C. Han, K.A. Willis, and J.F. Pierre. 2021. The gut mycobiome of healthy mice is shaped by the environment and correlates with metabolic outcomes in response to diet. *Commun. Biol.* 4:281. https://doi.org/10.1038/s42003-021-01820-z

Moyes, D.L., D. Wilson, J.P. Richardson, S. Mogavero, S.X. Tang, J. Wernecke, S. Höfs, R.L. Gratacap, J. Robbins, M. Runglall, et al. 2016. Candidalysin is a fungal peptide toxin critical for mucosal infection. *Nature*. 532: 64–68. https://doi.org/10.1038/nature17625

Narunsky-Haziza, L., G.D. Sepich-Poore, I. Livyatan, O. Asraf, C. Martino, D. Nejman, N. Gavert, J.E. Stajich, G. Amit, A. González, et al. 2022. Pan-cancer analyses reveal cancer-type-specific fungal ecologies and bacteriome interactions. *Cell*. 185:3789–3806.e17. https://doi.org/10.1016/j.cell.2022.09.005

Nash, A.K., T.A. Auchtung, M.C. Wong, D.P. Smith, J.R. Gesell, M.C. Ross, C.J. Stewart, G.A. Metcalf, D.M. Muzny, R.A. Gibbs, et al. 2017. The gut mycobiome of the Human Microbiome Project healthy cohort. *Microbiome*. 5:153. https://doi.org/10.1186/s40168-017-0373-4

Noble, S.M., B.A. Gianetti, and J.N. Witchley. 2017. *Candida albicans* cell-type switching and functional plasticity in the mammalian host. *Nat. Rev. Microbiol.* 15:96–108. https://doi.org/10.1038/nrmicro.2016.157

Ost, K.S., T.R. O'Meara, W.Z. Stephens, T. Chiaro, H. Zhou, J. Penman, R. Bell, J.R. Catanzaro, D. Song, S. Singh, et al. 2021. Adaptive immunity induces mutualism between commensal eukaryotes. *Nature*. 596:114–118. https://doi.org/10.1038/s41586-021-03722-w

Pappas, P.G., M.S. Lionakis, M.C. Arendrup, L. Ostrosky-Zeichner, and B.J. Kullberg. 2018. Invasive candidiasis. *Nat. Rev. Dis. Primers*. 4:18026. https://doi.org/10.1038/nrdp.2018.26

Petkau, A., M. Stuart-Edwards, P. Stothard, and G. Van Domselaar. 2010. Interactive microbial genome visualization with GView. *Bioinformatics*. 26:3125–3126. https://doi.org/10.1093/bioinformatics/btq588

Proux-Wéra, E., D. Armisén, K.P. Byrne, and K.H. Wolfe. 2012. A pipeline for automated annotation of yeast genome sequences by a conserved-synteny approach. *BMC Bioinformatics*. 13:237. https://doi.org/10.1186/1471-2105-13-237

Qin, J., R. Li, J. Raes, M. Arumugam, K.S. Burgdorf, C. Manichanh, T. Nielsen, N. Pons, F. Levenez, T. Yamada, et al. 2010. A human gut microbial gene catalogue established by metagenomic sequencing. *Nature*. 464:59–65. https://doi.org/10.1038/nature08821

Raimondi, S., A. Amaretti, C. Gozzoli, M. Simone, L. Righini, F. Candeliere, P. Brun, A. Ardizzoni, B. Colombari, S. Paulone, et al. 2019. Longitudinal survey of fungi in the human gut: ITS profiling, phenotyping, and colonization. *Front. Microbiol.* 10:1575. https://doi.org/10.3389/fmicb.2019.01575

Richardson, J.P., and D.L. Moyes. 2015. Adaptive immune responses to *Candida albicans* infection. *Virulence*. 6:327–337. https://doi.org/10.1080/21505594.2015.1004977

Ries, L.N.A., S. Beattie, R.A. Cramer, and G.H. Goldman. 2018. Overview of carbon and nitrogen catabolite metabolism in the virulence of human pathogenic fungi. *Mol. Microbiol.* 107:277–297. https://doi.org/10.1111/mmi.13887

Rosshart, S.P., J. Herz, B.G. Vassallo, A. Hunter, M.K. Wall, J.H. Badger, J.A. McCulloch, D.G. Anastasakis, A.A. Sarshad, I. Leonardi, et al. 2019. Laboratory mice born to wild mice have natural microbiota and model human immune responses. *Science*. 365:eaaw4361. https://doi.org/10.1126/science.aaw4361

Rosshart, S.P., B.G. Vassallo, D. Angeletti, D.S. Hutchinson, A.P. Morgan, K. Takeda, H.D. Hickman, J.A. McCulloch, J.H. Badger, N.J. Ajami, et al. 2017. Wild mouse gut microbiota promotes host fitness and improves disease resistance. *Cell*. 171:1015–1028.e13. https://doi.org/10.1016/j.cell.2017.09.016

Schoch, C.L., K.A. Seifert, S. Huhndorf, V. Robert, J.L. Spouge, C.A. Levesque, W. Chen, F.B. Consortium, F.B.C.A. List, E. Bolchacova, et al. 2012. Nuclear ribosomal internal transcribed spacer (ITS) region as a universal DNA barcode marker for Fungi. *Proc. Natl. Acad. Sci. USA*. 109: 6241–6246. https://doi.org/10.1073/pnas.1117018109

Shao, T.-Y., W.X.G. Ang, T.T. Jiang, F.S. Huang, H. Andersen, J.M. Kinder, G. Pham, A.R. Burg, B. Ruff, T. Gonzalez, et al. 2019. Commensal *Candida albicans* positively calibrates systemic Th17 immunological responses. *Cell Host Microbe*. 25:404–417.e6. https://doi.org/10.1016/j.chom.2019.02.004

Solis, N.V., and S.G. Filler. 2012. Mouse model of oropharyngeal candidiasis. *Nat. Protoc.* 7:637–642. https://doi.org/10.1038/nprot.2012.011

Sprague, J.L., L. Kasper, and B. Hube. 2022. From intestinal colonization to systemic infections: *Candida albicans* translocation and dissemination. *Gut Microbes*. 14:2154548. https://doi.org/10.1080/19490976.2022.2154548

Steinbiss, S., F. Silva-Franco, B. Brunk, B. Foth, C. Hertz-Fowler, M. Berriman, and T.D. Otto. 2016. Companion: A web server for annotation and analysis of parasite genomes. *Nucleic Acids Res*. 44:W29–W34. https://doi.org/10.1093/nar/gkw292

Thakker, P., M.W. Leach, W. Kuang, S.E. Benoit, J.P. Leonard, and S. Marusic. 2007. IL-23 is critical in the induction but not in the effector phase of experimental autoimmune encephalomyelitis. *J. Immunol.* 178: 2589–2598. https://doi.org/10.4049/jimmunol.178.4.2589

Underhill, D.M., and I.D. Iliev. 2014. The mycobiota: Interactions between commensal fungi and the host immune system. *Nat. Rev. Immunol.* 14: 405–416. https://doi.org/10.1038/nri3684

Vaas, L.A.I., J. Sikorski, B. Hofner, A. Fiebig, N. Buddruhs, H.-P. Klenk, and M. Göker. 2013. opm: An R package for analysing OmniLog(R) phenotype microarray data. *Bioinformatics*. 29:1823–1824. https://doi.org/10.1093/bioinformatics/btt291

Vautier, S., R.A. Drummond, K. Chen, G.I. Murray, D. Kadosh, A.J.P. Brown, N.A.R. Gow, D.M. MacCallum, J.K. Kolls, and G.D. Brown. 2015. *Candida albicans* colonization and dissemination from the GI tract. *Cell. Microbiol.* 17:445–450. https://doi.org/10.1111/cmi.12388

Vehkala, M., M. Shubin, T.R. Connor, N.R. Thomson, and J. Corander. 2015. Novel R pipeline for analyzing biolog phenotypic MicroArray data. *PLoS One*. 10:e0118392. https://doi.org/10.1371/journal.pone.0118392

Walker, B.J., T. Abeel, T. Shea, M. Priest, A. Abouelliel, S. Sakthikumar, C.A. Cuomo, Q. Zeng, J. Wortman, S.K. Young, and A.M. Earl. 2014. Pilon: An integrated tool for comprehensive microbial variant detection and genome assembly improvement. *PLoS One*. 9:e112963. https://doi.org/10.1371/journal.pone.0112963

Wang, Y., H. Chen, T. Xia, and Y. Huang. 2020. Characterization of fungal microbiota on normal ocular surface of humans. *Clin. Microbiol. Infect.* 26:123.e9–123.e13. https://doi.org/10.1016/j.cmi.2019.05.011

Wheeler, M.L., J.J. Limon, A.S. Bar, C.A. Leal, M. Gargus, J. Tang, J. Brown, V.A. Funari, H.L. Wang, T.R. Crother, et al. 2016. Immunological consequences of intestinal fungal dysbiosis. *Cell Host Microbe*. 19:865–873. https://doi.org/10.1016/j.chom.2016.05.003

Xu, R., Q. Li, H. Wang, Y. Su, and W. Zhu. 2023. Reduction of redox potential exerts a key role in modulating gut microbial taxa and function by dietary supplementation of pectin in a pig model. *Microbiol. Spectr.* 11: e0328322. https://doi.org/10.1128/spectrum.03283-22

Yamaguchi, N., K. Sonoyama, H. Kikuchi, T. Nagura, T. Aritsuka, and J. Kawabata. 2005. Gastric colonization of *Candida albicans* differs in mice fed commercial and purified diets. *J. Nutr.* 135:109–115. https://doi.org/10.1093/jn/135.1.109

Yeung, F., Y.-H. Chen, J.-D. Lin, J.M. Leung, C. McCauley, J.C. Devlin, C. Hansen, A. Cronkite, Z. Stephens, C. Drake-Dunn, et al. 2020. Altered immunity of laboratory mice in the natural environment is associated with fungal colonization. *Cell Host Microbe*. 27:809–822.e6. https://doi.org/10.1016/j.chom.2020.02.015

Zahradník, J., D. Dey, S. Marciano, L. Kolářová, C.I. Charendoff, A. Subtil, and G. Schreiber. 2021. A protein-engineered, enhanced yeast display platform for rapid evolution of challenging targets. *ACS Synth. Biol.* 10: 3445–3460. https://doi.org/10.1021/acssynbio.1c00395

Zangl, I., I.-J. Pap, C. Aspöck, and C. Schüller. 2019. The role of *Lactobacillus* species in the control of *Candida* via biotrophic interactions. *Microb. Cell*. 7:1–14. https://doi.org/10.15698/mic2020.01.702

Zeevi, D., T. Korem, A. Godneva, N. Bar, A. Kurilshikov, M. Lotan-Pompan, A. Weinberger, J. Fu, C. Wijmenga, A. Zhernakova, and E. Segal. 2019. Structural variation in the gut microbiome associates with host health. *Nature*. 568:43–48. https://doi.org/10.1038/s41586-019-1065-y

Zeevi, D., T. Korem, N. Zmora, D. Israeli, D. Rothschild, A. Weinberger, O. Ben-Yacov, D. Lador, T. Avnit-Sagi, M. Lotan-Pompan, et al. 2015. Personalized nutrition by prediction of glycemic responses. *Cell*. 163: 1079–1094. https://doi.org/10.1016/j.cell.2015.11.001

Supplemental material

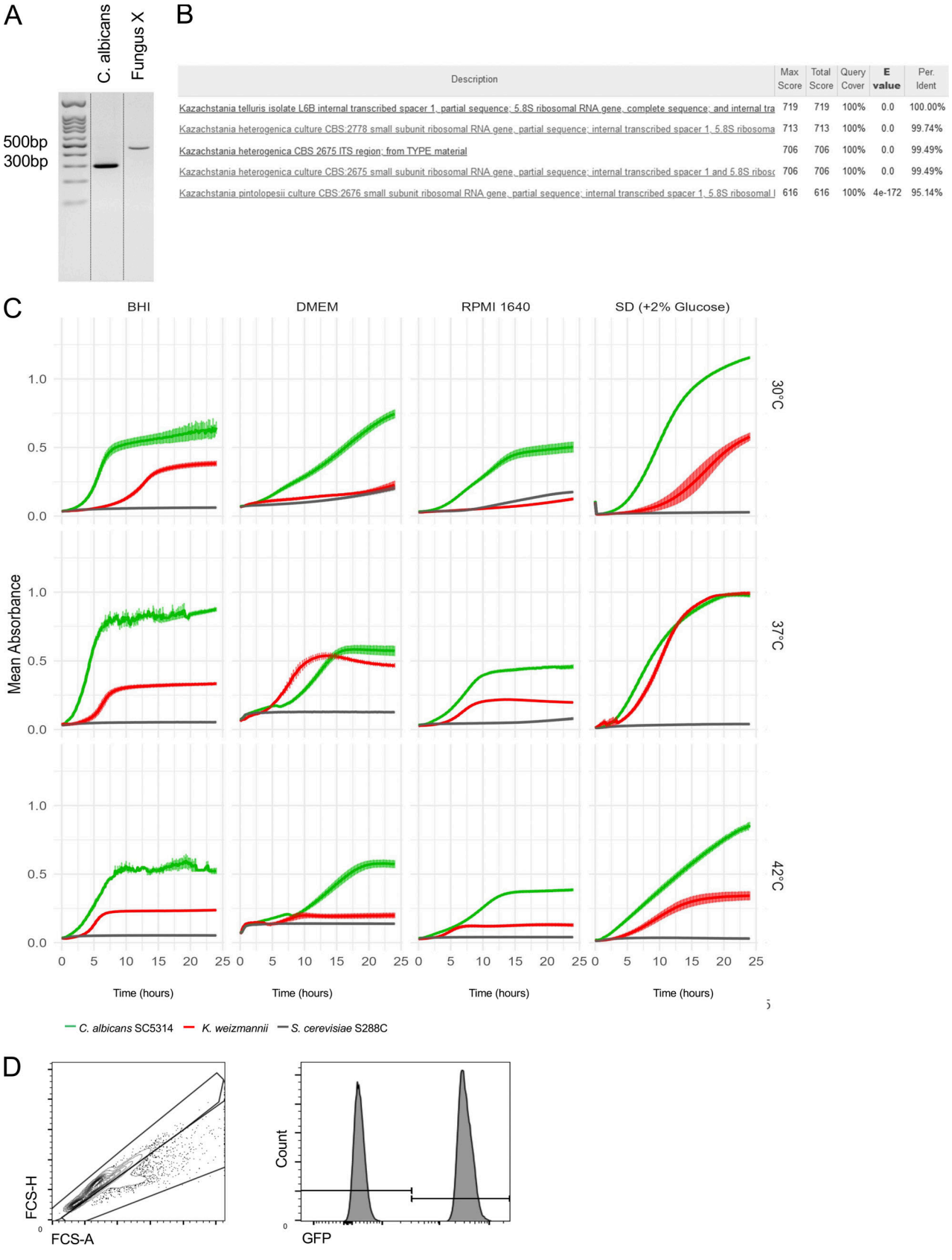

Figure S1. **Identification of novel fungal isolate and generation of *K. weizmannii* reporter strain. (A)** Gel analysis of PCR products amplifying ITS1 region of *C. albicans* and a fungal isolate. **(B)** Identification of novel fungal sp. based on ITS1 sequence. **(C)** Growth curves of *C. albicans*, *S. cerevisiae*, and *K. weizmannii* under different temperatures in indicated media, biological triplicates. **(D)** Example of flow cytometric analysis of mixed culture assay of *C. albicans* and *K. weizmannii* taking advantage of GFP expressing *C. albicans*. Source data are available for this figure: SourceData FS1.

A

ATGGCTAACTTGGACGAAATGTTGCAAACTACCGTTGAAGAAGTCA
GACAATTCTTGCAAGTTAATCGTGTCTTGGTGTTCCAATTTGAAGAG
GATTATTCCGGTGTTGTTGTTGTCGAAGCTGTTGATGATAGATGGC
AATCTATTTTGGGTACTCAAGTCAGAGACAGGTACTTCATGGAAACT
AGAGGTGAAGAATACTCCCATGGTAGATATCAAGCTATTGCCGATAT
CTACACTGCTAACTTGACTGAATGCTACAGAGAGTTGTTGGAACAA
TTTCAAGTTAGAGCCATTTTGGCCGTTCCAATCTTGCAAGGTAATCA
ATTGTGGGGTTTGTTGATTGCCCATCAATTGTCTGCTCCAAGACAA
TGGCAACCATGGGAAATTGATTTCTTGCAACAAATTGCTACCCAATT
GGCCATTGCTATTCAACAAGCT

B

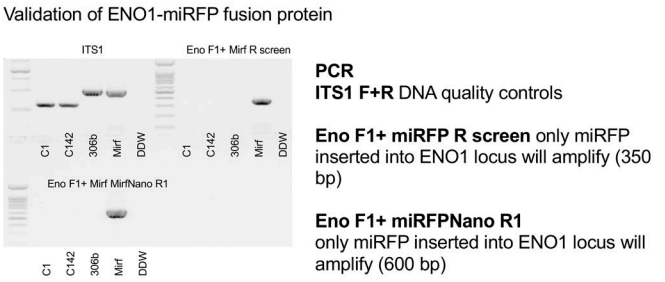

C

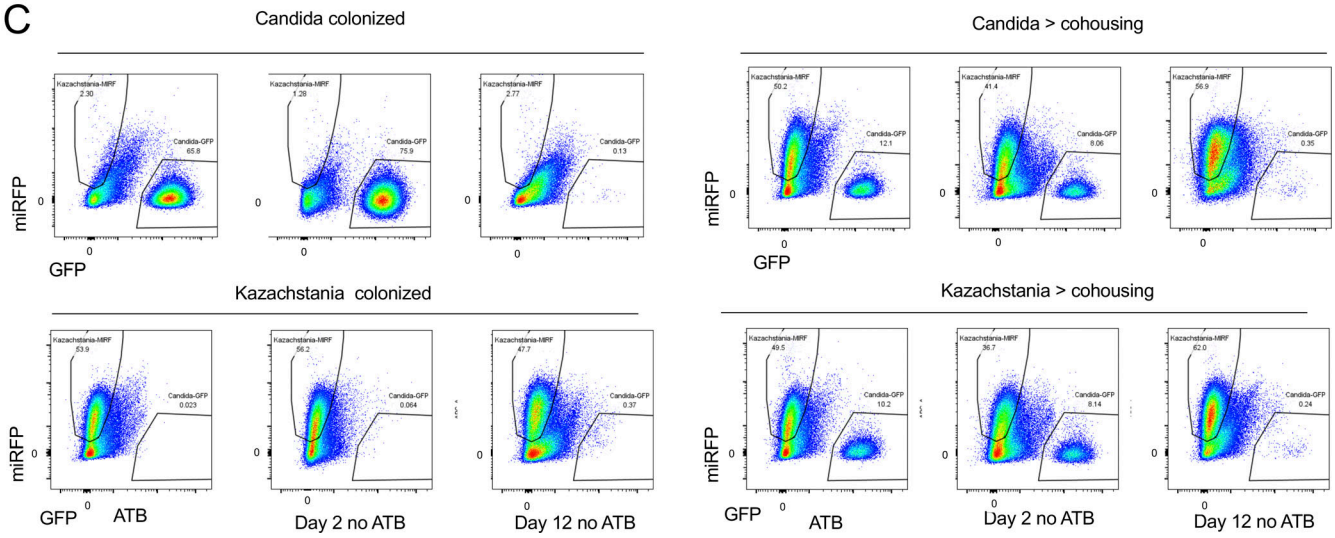

Figure S2. **Generation of *K. weizmannii* reporter strain. (A)** Sequence of modified fluorescent reporter miRFP670—further referred as miRFP. **(B)** PCR validation of proper insertion of miRFP into *K. weizmannii* genome and thus generation of ENO1-miRFP fusion protein. **(C)** Representative picture of recovery of *C. albicans* ENO1-GFP and *K. weizmannii* ENO1-miRFP from feces of single-colonized animals followed by cohousing (started as *Candida* or *Kazachstania*). Source data are available for this figure: SourceData FS2.

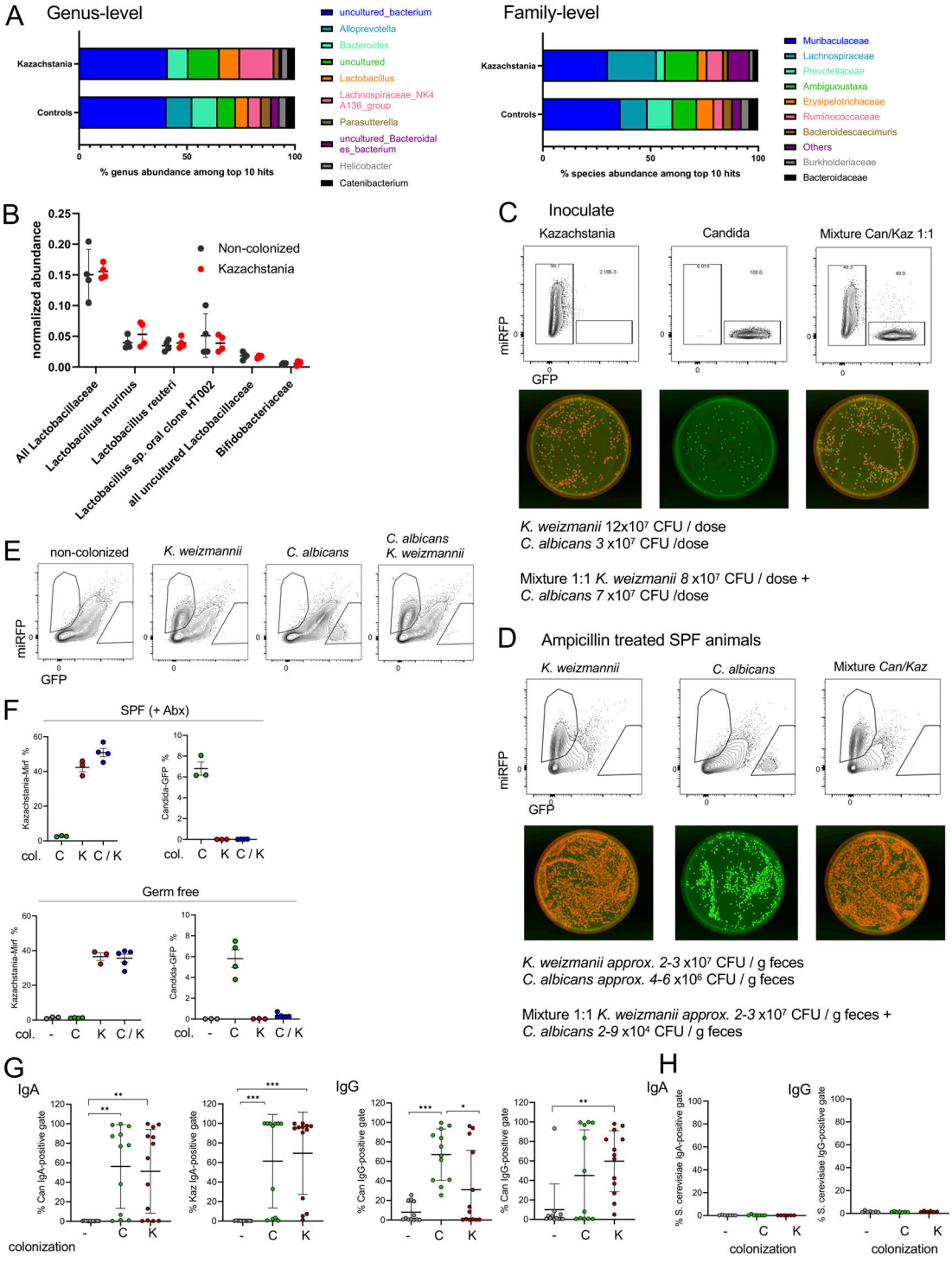

Figure S3. **Impact of *K. weizmannii* colonization on microbiome. (A)** Taxonomic composition of fecal bacteria identified in *K. weizmannii* colonized or non-colonized group (controls), as determined by 16S rRNA sequencing. The top 10 categories with the highest average relative abundance are shown at genus and family levels. **(B)** Normalized abundance of fecal Lactobacillaceae (divided into specific *Lactobacilli* species) and Bifidobacteriaceae, determined by 16S sequencing. **(C and D)** In vivo competition between *C. albicans* and *K. weizmannii* upon co-administration in germ-free animals and in Abx-treated WT mice: FACS and cultivation analysis of culture inoculate for oral administration (C) Representative picture of recovery of *C. albicans* ENO1-GFP and *Kazachstania* ENO1-miRFP from feces of colonized animals using flow cytometry and cultivation (D). **(E)** Flow cytometric analysis of feces of germ-free animals 1 wk after oral inoculation of single fungi cultures or mixed *C. albicans* SC5314 (ENO1-GFP)/*K. weizmannii* (ENO1-miRFP) culture. **(F)** Percentages of *C. albicans* and *K. weizmannii* recovered from feces of germ-free animals colonized with *C. albicans* SC5314 (C), *K. weizmannii* (K), or mixed culture (C/K) compared with Abx-treated SPF animals 1 wk after administration as determined by flow cytometry analysis (K); representative of two independent experiments. **(G)** Graph summarizing results serum reactivity of *C. albicans*– or *K. weizmannii*–colonized animals (data shown in Fig. 4 C). Y axis represents percentage of anti-IgA or IgG-positive gate with mean ± SEM, *N* = 11–13 mice per group. **(H)** Summary of flow cytometric analysis of humoral IgA and IgG anti-fungal reactivity for cultured *S. cerevisiae*, using sera for which anti-*C. albicans* or *K. weizmannii* reactivity was shown in Fig. 4 C. * P ≤ 0.05, ** P ≤ 0.01, *** P ≤ 0.001.

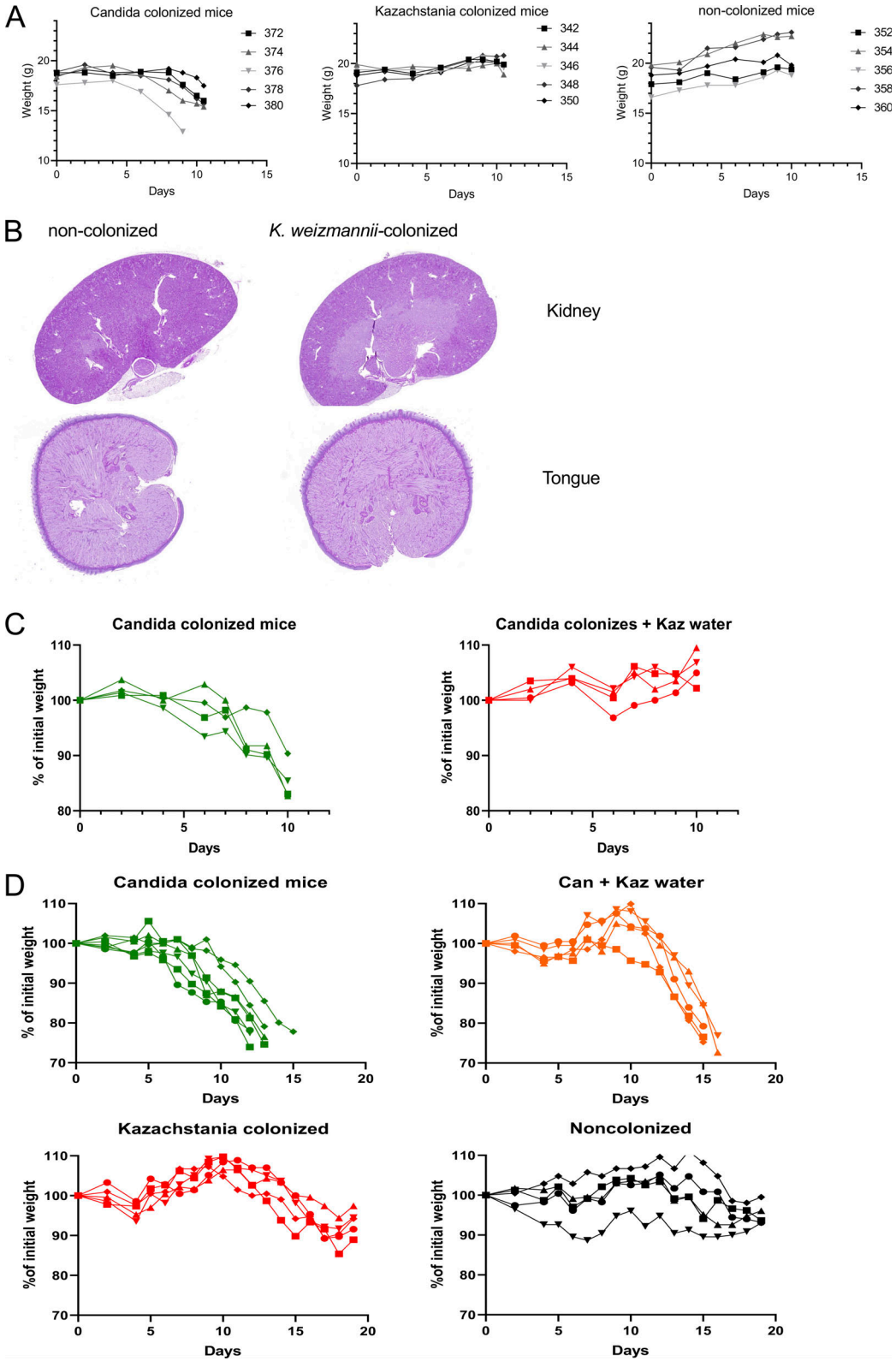

Figure S4. **Analysis of *C. albicans*–colonized immunosuppressed animals and of *K. weizmannii* and *C. albicans*–colonized immunosuppressed animals.** **(A)** Absolute weight monitoring (g) of individual mice in *C. albicans* colonization, *K. weizmannii*–colonized and non-colonized group upon immunosuppressive treatment. **(B)** Representative picture of kidneys and tongues (PAS staining) of immunosuppressed non-colonized and *Kazachstania*-colonized animals in end time point (day 10). **(C)** Absolute weight (g) monitoring, comparison of immunosuppressed animals following *C. albicans* colonization and *K. weizmannii*–outcompeted *C. albicans* colonization, monitoring till the end of experiment (day 10). **(D)** Absolute weight (g) monitoring showing the prolonged course of immunosuppressive treatment (mice sacrificed upon >20% weight loss), comparison of immunosuppressed animals following *C. albicans* colonization and *K. weizmannii*–outcompeted *C. albicans* colonization, and *K. weizmannii*–colonized and non-colonized animals.

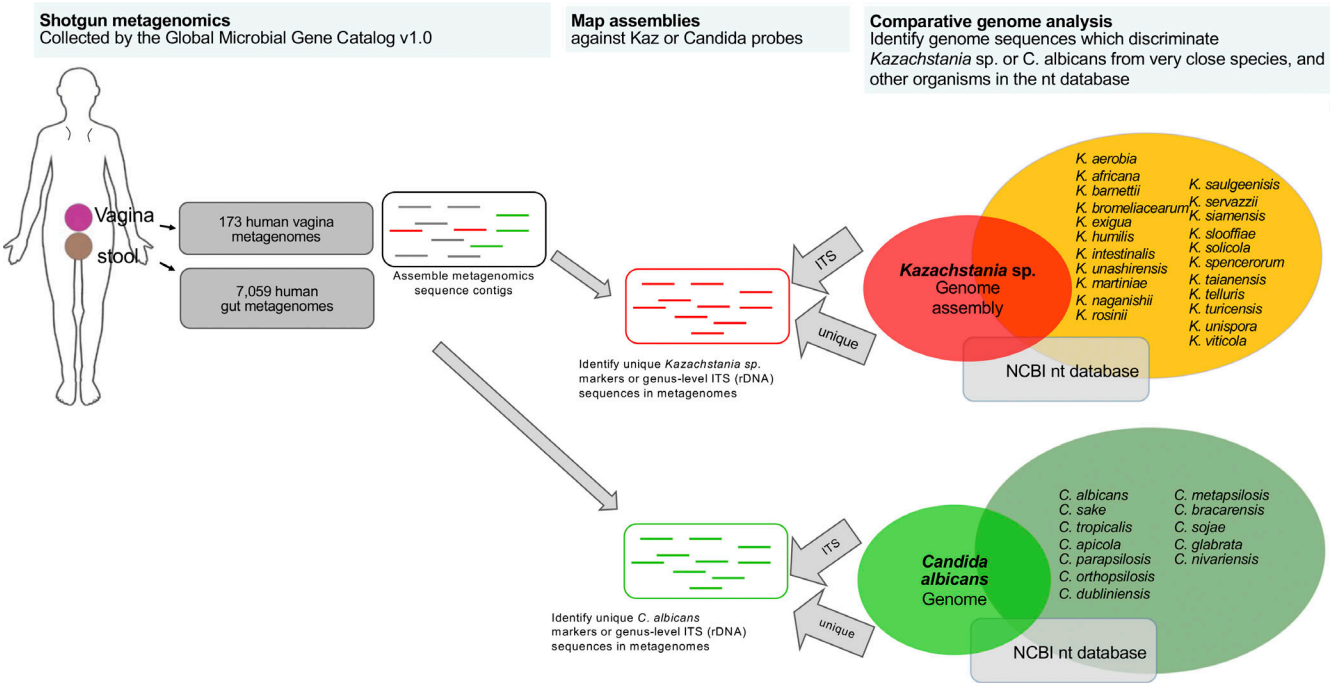

Figure S5. **Human metagenomes identified with *K. weizmannii*.** Schematic of bioinformatic screening strategy of metagenomes. Briefly (from right to left), comparative genome analysis identified nucleotide regions that are unique to the genomes of either *K. weizmannii* or *C. albicans* species, together with genus-level regions of their ITS sequences. These regions were used to screen thousands of shotgun metagenomics collected and assembled by the Global Microbial Gene Catalogue v1.0 (Coelho et al., 2022) (see Materials and methods).

Provided online are Table S1, Table S2, Table S3, Table S4, Table S5, Table S6, Table S7, Data S1, Data S2, and Data S3. Table S1 lists *Kazachstania* genomes used for sequence searches. Table S2 lists *Candida* genomes used for sequence searches. Table S3 lists the *Kazachstania* clade tree. Table S4 lists the yeast family tree. Table S5 shows metadata and read counts of 32 metagenomes from human gut origin, in which *K. weizmannii* was identified. Table S6 shows metadata and read counts of 22 metagenomes from human vaginal origin, in which either *K. weizmannii* or *C. albicans* were identified. Table S7 shows classification of percent of raw reads to species level used in this study. Data S1 shows raw data of Biolog assay. Data S2 shows raw data for growth curves. Data S3 shows raw data for EC damage assay.